

## Gross Brukkaros - The unusual intracaldera sediments and their magmatic components

T. Stachel<sup>1\*</sup>, G. Brey<sup>2</sup> & I.G. Stanistreet<sup>3</sup>

<sup>1</sup>Institut für Geologie, Universität Würzburg, Pleicherwall 1, 97070 Würzburg, Germany

<sup>2</sup>Max Planck Institut für Chemie, Abt. Kosmochemie, Saarstraße 23, 55122 Mainz, Germany

<sup>3</sup>Department of Geology, University of the Witwatersrand, P. Bag 3, Wits 2050, South Africa

\*present address: Department of Geology and Applied Geology, University of Glasgow, Glasgow G12 8QQ, United Kingdom

Gross Brukkaros, Namibia, is a broad (10 km diameter) dome structure in Nama Group country rocks, with a crater-shaped central depression. Formation of the dome structure has recently been attributed to a shallow intrusion, which subsequently became partly depleted during volcanic activity in the Brukkaros Volcanic Field, causing cauldron subsidence. The subsiding depocentre became filled by a sedimentary sequence corresponding to alluvial fan delta / lacustrine environments. Here we give a detailed petrographical and chemical description of the Brukkaros sediments and their lithic and mineral constituents. As main sources for the Brukkaros sediments we identified shales, cherts, sandstones, and quartzites from Karoo Sequence and Nama Group rocks as well as Karoo dolerites. A contribution of aeolian deposits (early Kalahari?) is also identified. No primary pyroclastic deposits were found within the Brukkaros depocentre. Volcanogenic fragments in the form of carbonatitic lapilli, however, are described from the Brukkaros sediments for the first time and are attributed to redeposition of tephra deposits of the common carbonatitic diatremes at and around Brukkaros. Basement fragments within the Brukkaros sediments might well have been derived from the same source. Metasomatic-hydrothermal alteration and cementation of the Brukkaros rocks can be shown to have operated already during sedimentation. Metasomatic alkali feldspar compositions indicate that fenitization took place mainly at subsolvus temperatures.

### Introduction

Gross Brukkaros is a cone-shaped inselberg about 600 m in height located in the Namaland plain of southern Namibia between Mariental and Keetmanshoop (Fig. 1). The base of the hill has a diameter of about 7 km, the crater-shaped central depression measures about 3 km in diameter (Fig. 2). Structurally Gross Brukkaros comprises a ring-shaped anticlinal structure within late Precambrian to Cambrian Nama Group sediments. Earlier studies (e.g. Janse, 1969; Miller and Reimold, 1987) interpreted Gross Brukkaros as a large diatreme. Stachel *et al.* (1993, 1994) attribute doming of the country rocks to the shallow intrusion of a laccolith shaped alkaline or carbonatitic magma body. Subsequent depletion of the reservoir during volcanic activity around and within(?) Gross Brukkaros led to cauldron subsidence with the evolution of the centrally located depocentre. From contact relationships (Stachel *et al.*, 1994) the formation of the depocentre can be related temporally with the volcanic activity of the surrounding carbonatitic and kimberlitic Gibeon Volcanic Province of Upper Cretaceous age (Reid *et al.*, 1990; Davies *et al.*, 1991). This relationship in age is supported by newly discovered plant fossils (Kelber *et al.*, 1993) within the Brukkaros sediments, which suggest deposition during the Upper Cretaceous or later.

The subsiding Brukkaros depocentre was filled by a sequence consisting mainly of debris flow and mudflow deposits with minor fluvial (braided channel) and lacustrine sediments. Stachel *et al.* (1994) reconstructed the sedimentary environment in terms of a set of coalesced alluvial fans passing centrally into a permanent lake with fluctuating water level, with facies akin to those which form on an alluvial fan delta.

Cauldron subsidence was a continuous process dur-

ing sedimentation since bedding angles of 20-30° for the sediments clearly are not depositional angles. This especially applies to lake beds which would have been deposited primarily on a more or less horizontal lake floor.

The Brukkaros deposits were subjected to a metasomatic-hydrothermal alteration process (Ferguson *et al.*, 1975; Miller and Reimold, 1987) which led to silicification of the sediments. This made the Brukkaros sediments highly resistant to weathering with the consequence that Gross Brukkaros remains as a cone-shaped inselberg, which has previously been misidentified as



Figure 1: Location of Gross Brukkaros in southern Namibia (dashed lines = major roads). Diamonds indicate the extent of the Gibeon Kimberlite Province.

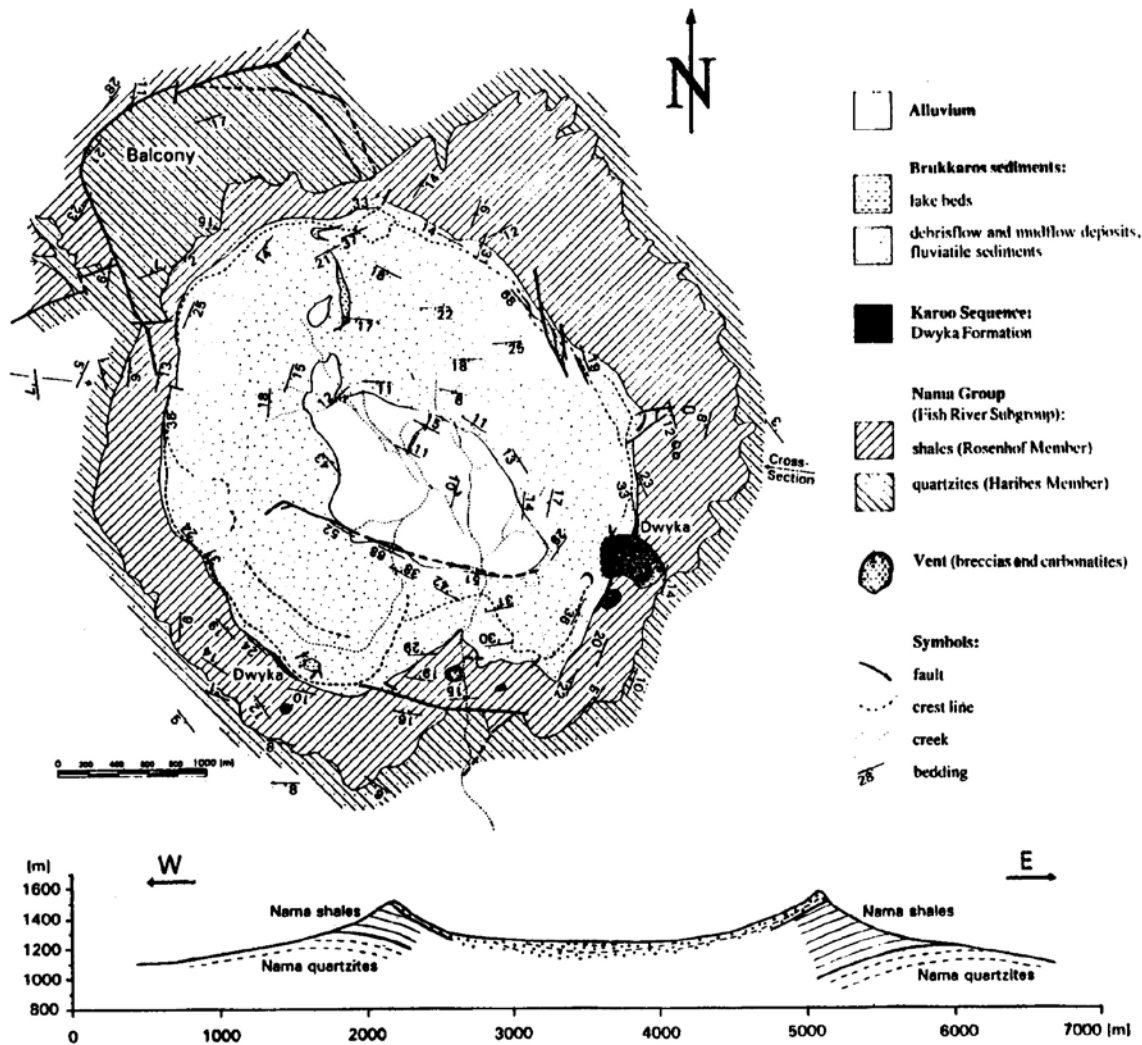


Figure 2: Geological map of Gross Brukkaros after Stachel *et al.* (1994).

an original volcanic cone.

One of the main paradoxes of Gross Brukkaros is that its shallow level magmatic origins should be so sparsely represented in its caldera-fill. This makes it an important end member in the spectrum of caldera types. For this reason it is important that the petrography and chemistry of the Brukkaros sediments and their lithic and mineral constituents should be recorded in detail. The aim of the present work is, therefore, to identify possible sources for the mineral constituents, to characterize the chemistry of the volcanoclastic components within the Brukkaros sediments, and to describe the effects of secondary metasomatic-hydrothermal alteration.

### Methods

#### Microprobe Analyses

Microprobe analyses were carried out with a CAMECA SX-50, equipped with four spectrometers. Element concentrations were determined by wavelength-disper-

sive spectrometry (WDS) using the GEO option of the CAMECA software (with PAP correction). Accelerating voltage was 15.0 kV, beam current 10.0 nA. Measuring times, detection limits, and standards used are given in Table 1.

Since Ba was analyzed at the  $L\alpha$  line it is only reported for Ti-free (peak overlap) analyses.

Detection limits for mineral and matrix analyses were calculated from typical analyses for each data set ( $d.l. = 3 * (\text{background intensity})^{1/2}$ ).

#### Modal Analyses

Petrographic descriptions are based on examination of about 50 thin-sections of the Brukkaros sediments. Additional information comes from grain mounts of heavy mineral and magnetic separates from a sample taken at the base of the upper waterfall, within the prominent gully ("Entrance Valley") on the south side of Brukkaros. The sample gives an average of the material washed into the Brukkaros "crater", which is solely

Spectrometer 1 TAP	Spectrometer-2 PET	Spectrometer 3 PET	Spectrometer 4 LIF
Na (20sec., Albite)	Ca (20 sec., Wollast.)	K (20 sec., Orthocl.)	Fe (40 sec., Fe <sub>2</sub> O <sub>3</sub> )
Sr (120 sec., SrSO <sub>4</sub> )	Ti (40 sec., MnTiO <sub>3</sub> )	Mn (40 sec., MnTiO <sub>3</sub> )	Zn (120 sec., ZnS)
Mg (20 sec., MgO)	Ba (40 sec., BaSO <sub>4</sub> )	Cr (120 sec., Cr <sub>2</sub> O <sub>3</sub> )	
Si (20 sec., Orthocl.)	Nb (120 sec., Nb)		
Al (20 sec., Al <sub>2</sub> O <sub>3</sub> )			
P (20 sec., Apatite)			

**Table 1:** Analytical conditions for microprobe analyses. Counting times on peak and standards used for calibration (from the Cameca standard set). Accelerating voltage: 15.0 kV. Beam current: 10.0 nA. Background time: peak time. Background offset: +500 and -500; Sr +500 and -1000. Ba, Sr and Nb: L $\alpha$ ; others: K $\alpha$ .

derived from the Brukkaros sediments.

Modal analysis of 19 thin-sections were carried out with an automatic point counter (Swift, model F). 1000 points were counted on a surface of 7-10 cm<sup>2</sup>. Since the optical distinction between buff coloured juvenile lapilli and reworked Brukkaros material is often highly uncertain, lapilli contents were excluded and recalculated after point counting. Rare accessories, like tourmaline or garnet, are also not reported.

### Composition of Brukkaros sediments

#### Types of sediments

Stachel *et al.* (1994) identified four principal facies associations within Gross Brukkaros:

1. The matrix-supported gravel/sandstone association comprises a variety of rocks ranging from massive mudstones at the one end to matrix-supported breccias at the other end. Their origin is attributed to deposition from debris flows and mudflows, which usually dominate sedimentation in proximal alluvial fan environments.

2. The clast supported gravel and sandstone association consists of plane bedded and trough cross-bedded sandstones with intercalated pebble and cobble breccias. This association represents channelized fluvial deposition on the fan, with the coarser massively bedded intercalations interpreted as gravel bars.

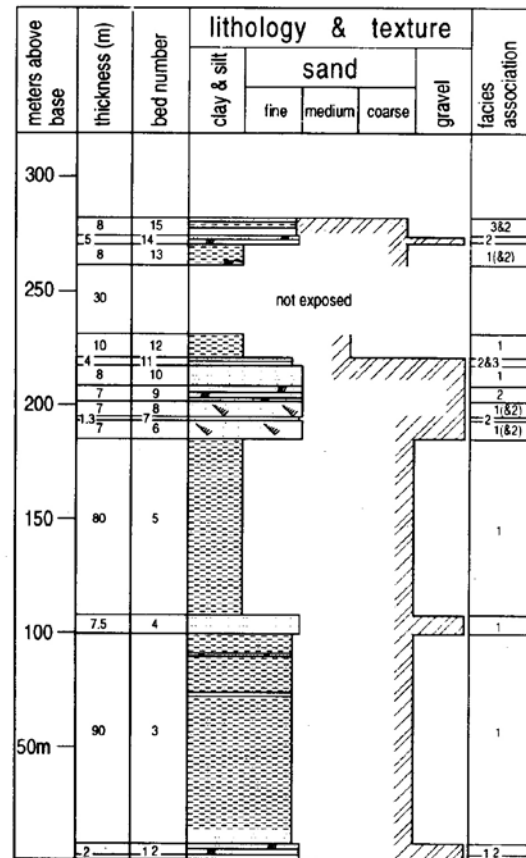
3 and 4. Interbedded mudstones and sandstones occur in a marginal and in a central facies association. Within the central facies association (4) normally graded turbiditic sand- and mudstones are interbedded with laminated mudstones. Facies association 3 represents an interbedding of these lake deposits with coarser sediments otherwise typical for associations 1 and 2, thus reflecting the facies transitions at the lake margins.

Stachel *et al.* (1994) for the first time recognized juvenile carbonatitic lapilli within the Brukkaros depos-

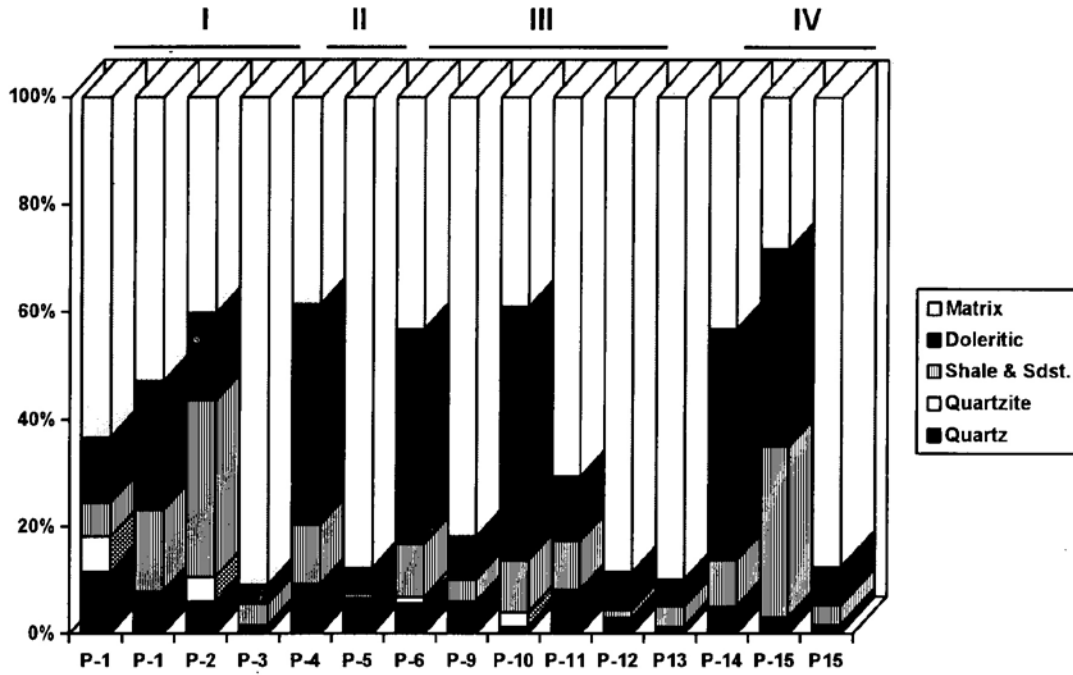
its. Their characteristics and chemical composition are given later in the paper. Although these lapilli may form a major rock constituent, primary pyroclastic deposits (Janse, 1969) are not exposed at Brukkaros.

Fig. 3 is a measured section through the Entrance Valley at the south side of Brukkaros. It shows the dominance of debris flow and mudflow deposits (association 1) over fluvial sediments (2). In this section lake beds occur only in the marginal facies association (3). However, lake beds of the central facies association (4) occur in several scattered outcrops along the "crater" rim and the inner slopes of Brukkaros.

From Fig. 3 several fining upwards sequences can be recognized (layer 1-3,4-5,6-12 (or 13?), and 14-15). These sequences have been interpreted as cycles of deposition, beginning with rapid deposition of sediments rich in quartz, shale, and disintegrated Karoo dolerite (plagioclase and clinopyroxene). These sediments result from enhanced incision into the crater walls (Stachel *et al.*, 1994). The sediments become increasingly dominated by fine-grained deposits towards the top of each cycle. The cyclicity in sedimentation has been attributed to reactivation of the system during repeated phases of subsidence within the caldera, although climatic changes may also provide a second-



**Figure 3:** Measured section of the Brukkaros sedimentary sequence as exposed in the Entrance Valley at the south side of the structure.



**Figure 4:** Modal variations of the five principal constituents of the Brukkaros sediments in the Entrance Valley section (Fig.3). "Doleritic" summarizes small dolerite fragments as well as plagioclase and clinopyroxene grains. "Quartzite" represents all the coarser polycrystalline quartz fragments.

ary cause controlling facies changes.

Fig. 4 shows the results of modal thin-section analysis for the measured section within the Entrance Valley. Only one thin-section per unit was counted in these partly very in homogeneous units, but the increasing matrix-contents and correspondingly decreasing crystal and lithic fragment contents clearly follow the observed cyclicity.

*Constituents*

*Quartz*

Detrital, monocrystalline quartz grains are major con-

stituents with contents of 5-15 vol% in most Brukkaros sediments. Only some of the fine-grained mudflow units and some gravel-bearing arkoses (mainly reworked doleritic material) contain less than 1 % quartz grains. Most quartz grains fall in between fL and mU (i.e. 125-500 μ), with a maximum range from about 50-800 μ. Rounded to subrounded quartz grains with intermediate sphericity prevail, subangular grains also occur.

About 10-20% of the quartz grains are well rounded and show a high sphericity (Fig. 5). Their average grain size is about 300 μ (mL) as measured in thin section with a range between 125-500 μ. Several show a coating of haematite ( 1-10 μ thick), which may also be ob-

Strat. Column	P-1	P-1	P-2	P-3	P-4	P-5	P-6	P-9	P-10	P-11	P 12	P13	P14	P-15
Sample No.	GB91	GB92	GB92	GB92										
	-78	-1	-77	-67	-55	-60	-75	-74	-73	-32	-70	-6	-8	-11
Quartz Grains	11	7	6	1.4	9	6	6	6	1.3	8	3.0	1.3	4	3
Plagioclase	7	8	7	1.9	19	3	12	5	23	8	4	4	21	18
Cpx	4	14	4	1.1	16	1.4	22	2	17	3	2	1.0	9	9
Dolerite Frag.	0.9	2	5	0.4	6	0.6	6	1.0	7	0.9	0.5	0	7	9
Oxide Phases	1.8	1.0	0.1	0.8	0	0.4	0.7	0.1	0.1	0.9	0.1	0.2	0.2	0.1
Microcline	0.2	0.7	0	0.2	0.8	0.3	0.3	0.1	0.8	0.4	0.6	0.9	0.5	0.7
Carb. Rhomb.	0.4	35	1.7	0	0.3	0	1.5	0	10	25	1.7	0	0	0
Quartzite	7	0.3	5	0.1	0.3	0.6	1.1	0.2	3	0.2	0	0	0	0
Shale & Sdst.	6	15	33	4	11	0.9	10	4	10	9	1.3	4	19*	32
Matrix	61	16	38	90	38	87	41	82	28	45	86	89	38	28

\*11% of 19% are clasts of reworked Brukkaros material

**Table 2:** Modal composition of the Brukkaros sediments from point counting of thin sections. P1-P15 refers to layers within the measured section (Fig.3).

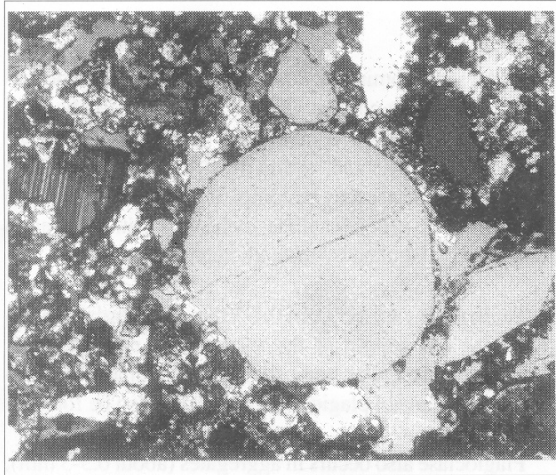


**Figure 5:** Well rounded and highly spherical quartz grain (0.45 mm), coated by haematite. Quartz cement at the lower right hand corner of the grain has the same crystallographic orientation as the sand grain and includes euhedral calcite at its edges. A fresh, angular plagioclase grain can be recognized by its well developed polysynthetic twinning. Sample GB91-45, NW-rim of Brukkaros, picture width: about 1 mm, crossed nichols.

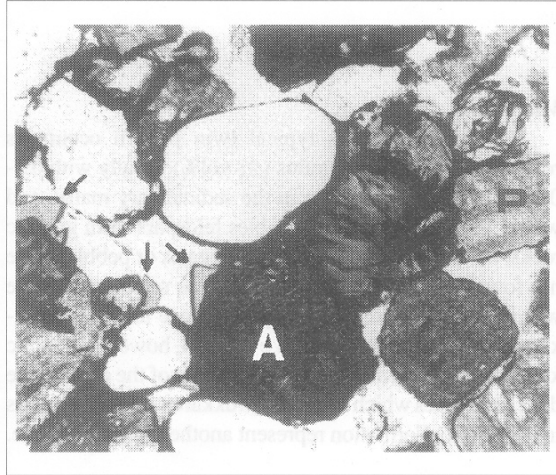
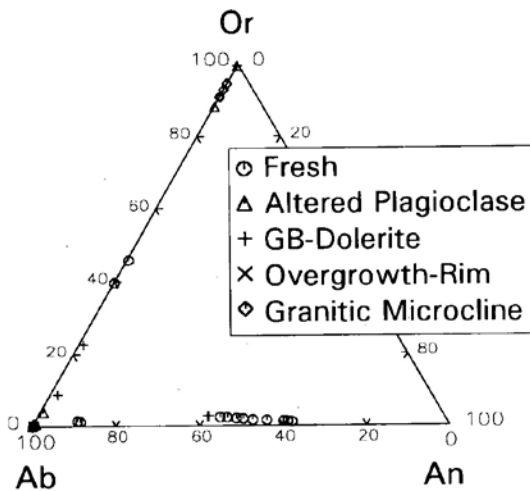
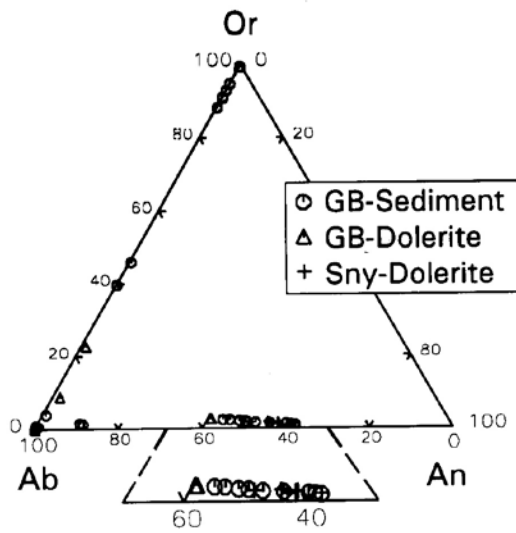


**Figure 7:** Sandstone consisting of oxidized and altered augite (A), altered plagioclase (P), and quartz with a strong haematite coating. The intergranular space is cemented by clear quartz. Euhedral aegirine (arrows) grows on a quartz grain and on the altered augite into the cemented area. Sample GB92-2, fluvatile deposited sandstone, Entrance Valley, profile layer P2 (Fig.3), picture width: about 1.5mm.



served on less well rounded grains. Such quartz grains with high textural maturity are most probably derived from aeolian transported sediments, i.e. dune sands.

*Feldspar*

*Microcline*

Microcline with its typical twin pattern occurs as rounded to subrounded grains ( $\leq 1$  vol%) usually with 0.1-0.2 mm and up to 0.5, mm in the sedimentary matrix and within juvenile lapilli. It resembles feldspars from granitic rocks, although granitic crystal aggregates or pebbles were not found in thin-sections of Brukkaros sediments. There was no granitoid basement exposed close to Gross Brukkaros during its formation and evolution, however, granitic xenoliths are extremely common in some of the carbonatite dykes and pipes which surround Brukkaros. Granitoid clasts in the Dwyka Formation represent another possible source.

*Plagioclase*

In the sand-dominated debris flow and fluvatile deposits the plagioclase content varies from 5% up to about 35 vol%. The fine grained mudflows have low

**Figure 6a:** Microprobe analyses of feldspar plotted in the system orthoclase-albite-anorthite (GB-Sediment: individual feldspar crystals and small doleritic plagioclase-clinopyroxene aggregates from the Brukkaros sediments; GB-Dolerite: feldspar from a larger, metasomatized dolerite pebble in Brukkaros sandstone; Sny-Dolerite: plagioclase from the Snyfontein dolerite sill)

**Figure 6b:** Feldspar analyses from Gross Brukkaros only. See text for explanation of data groups.

plagioclase contents (1-2 vol%) and, within the fine grained lacustrine deposits, plagioclase may be completely absent. Plagioclase also occurs as xenocrystalline inclusions within juvenile lapilli, partly resorbed by the carbonate matrix.

Grain sizes vary between 0.1-1 mm in accordance with grain size and sorting of the surrounding rock material. Angular to subangular grain shapes predominate, but subrounded to rounded plagioclase grains can also be found.

Plagioclase also occurs in aggregates (about 0.5-3 mm), which may be monomineralic or polymineralic with pyroxene. Within these aggregates plagioclase ranges from 0.4-1 mm, but coarser and finer grained

varieties of such dolerite clasts also exist.

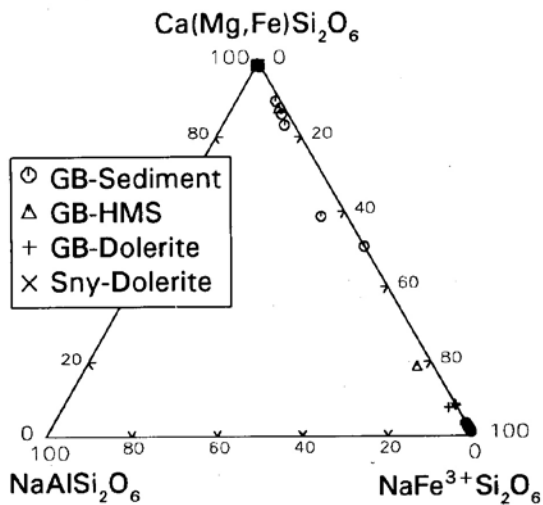
Both fresh and altered plagioclase can be observed within aggregates and as individual grains.

*Feldspar Chemistry*

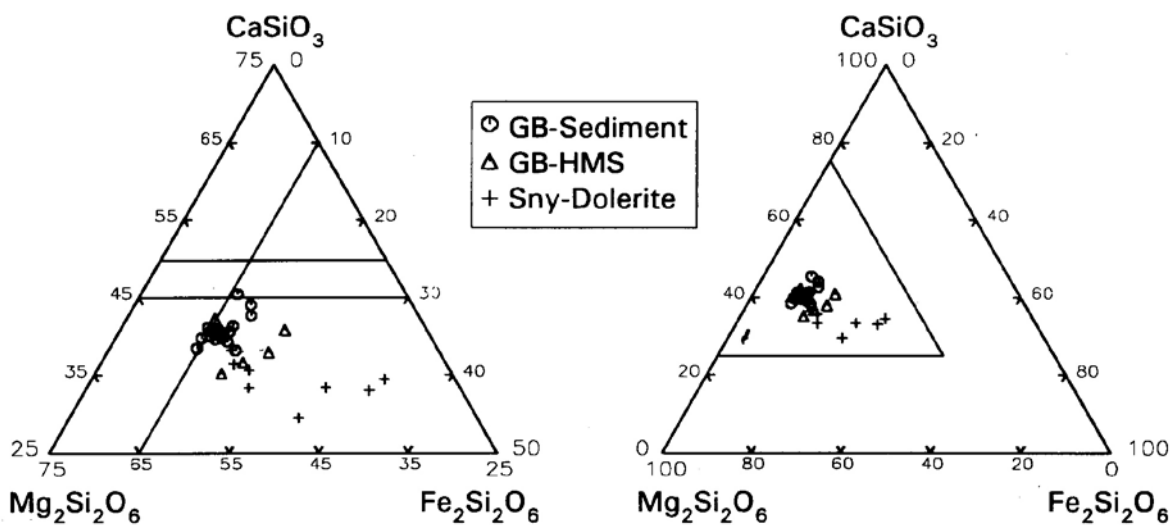
Figure 6a is a comparison of feldspars from Gross Brukkaros and those from the Snyfontein dolerite sill (exposed beside the gravel district road 609 from Keetmanshoop to Berseba). Plagioclase from Snyfontein ranges between An 50-60 with a weakly developed normal zoning of decreasing An and increasing Fe from core to rim (see Tab. 3). Plagioclase from the Brukkaros sediments overlap completely those from Snyfontein but almost pure albite also occurs. In addition alkali feldspars ranging from pure K-feldspar to pure albite are also observed.

Figure 6b groups the feldspar data from Brukkaros into (i) apparently fresh crystals, (ii) altered feldspar identified as former plagioclase from twin lamellae, (iii) plagioclase and its alteration products from a dolerite pebble (3 cm in diameter), (iv) albite overgrowth rims on plagioclase, and (v) microcline with well developed twinning indicating a granitic origin.

Fresh plagioclase from the Brukkaros sediments varies between An 40-60. Altered plagioclase plots not only in the albite corner, but also along the join albite-orthoclase and at pure K-feldspar. Plagioclase altered to pure K-feldspar was also observed within the metasomatized dolerite pebble. Potassic alkali feldspar-quartz symplectites (typical for granophyres) were observed as single grains and within doleritic plagioclase-clinopyroxene aggregates. Single symplectite grains may therefore stem from either granophyres or from dolerites. Overgrowth rims on altered plagioclase plot in the albite corner. Pure albite also occurs as small rounded to subhedral grains and may either represent a product of metasomatism or a detritic input from an additional



**Figure 8a:** Pyroxene analyses from Gross Brukkaros (whole rock and heavy mineral samples) and the Snyfontein dolerite sill plotted in a diagram augite-jadeite-acmite (Clark and Papike, 1968).



**Figure 8b:** Primary pyroxene analyses (i.e. acmite <5 mol%) from Gross Brukkaros and Snyfontein plotted in the system wollastonite-clinoenstatite-clinoferrrosilite.

Sample Code	SNY92-1 Z4-2A	SNY92-1 Z4-3B	GB91-77 P7-10a	GB92-4 21	GB91-43 4	GB91-73 GK-15	GB91-77 P6-9a	GB91-44 P7-14a	GB91-44 P7-14b
Remark	Dolerite	Dolerite	Plag - Cpx Aggregate	Dolerite Pebble	Sediment. Matrix	Plag - Cpx Aggregate	Plag - Cpx Aggregate	Sediment. Matrix	Sediment. Matrix
Mineral	Plagioclase Core	Plagioclase Rim	Plagioclase Core	Plagioclase Core	Albite subhedral	Albite Beam 30	K-Feldspar	Plutonic Microcline	Plutonic Microcline
SiO <sub>2</sub>	53.6	53.6	52.8	58.3	69.0	67.7	65.5	64.7	65.1
Al <sub>2</sub> O <sub>3</sub>	28.4	28.0	29.2	25.4	19.6	19.1	17.8	18.5	18.5
MgO	0.06	<0.05	0.05	<0.05	<0.05	0.05	<0.05	<0.05	<0.05
CaO	12.0	11.8	12.7	8.44	0.10	0.12	<0.05	<0.05	<0.05
FeO	0.51	0.83	0.76	0.60	0.15	0.49	<0.07	<0.07	<0.07
MnO	<0.05	<0.05	<0.05	0.07	<0.05	<0.05	<0.05	<0.05	<0.05
BaO	0.09	<0.05	<0.05	0.05	<0.05	<0.05	<0.05	0.22	0.09
Na <sub>2</sub> O	4.72	4.97	4.24	6.46	11.9	11.3	0.06	1.00	1.00
K <sub>2</sub> O	0.31	0.23	0.20	0.48	0.06	0.12	16.7	15.2	15.4
total	99.6	99.4	99.9	99.9	100.9	98.9	100.1	99.6	100.1
Si	2.442	2.451	2.402	2.625	2.992	2.995	3.025	2.995	2.996
Al	1.524	1.507	1.569	1.348	1.003	0.996	0.970	1.008	1.004
Mg	0.004	0.000	0.003	0.000	0.000	0.003	0.000	0.000	0.000
Ca	0.586	0.576	0.617	0.407	0.005	0.005	0.000	0.000	0.000
Fe <sup>2+</sup>	0.020	0.032	0.029	0.023	0.006	0.018	0.000	0.000	0.000
Mn	0.000	0.000	0.000	0.003	0.000	0.000	0.000	0.000	0.000
Ba	0.002	0.000	<.000	0.001	0.000	0.000	0.001	0.004	0.002
Na	0.417	0.440	0.374	0.563	0.999	0.972	0.005	0.090	0.089
K	0.018	0.014	0.012	0.028	0.003	0.007	0.983	0.897	0.904
total	5.013	5.019	5.006	4.997	5.007	4.996	4.984	4.994	4.996
[O]	8.000	8.000	8.000	8.000	8.000	8.000	8.000	8.000	8.000
Or	0.018	0.014	0.012	0.028	0.003	0.007	0.995	0.909	0.910
Ab	0.408	0.427	0.373	0.564	0.992	0.988	0.005	0.091	0.090
An	0.574	0.559	0.615	0.408	0.005	0.005	0.000	0.000	0.000

**Table 3:** Microprobe analyses from Gross Brukkaros and the Snyfontein dolerite sill. Analyses 1 and 2 represent a core/rim pair of a plagioclase from Snyfontein.

crystalline source as yet not recognized.

The two data points close to the middle of the Or-Ab join are also of uncertain origin, since the apparently relatively fresh crystals exhibit polysynthetic twinning indicative of plagioclase.

The alteration of plagioclase at Gross Brukkaros may be a result of: (i) Na-metasomatism, so that plagioclase of doleritic origin with its intermediate An-contents became altered into and/or overgrown by albite. (ii) continued K-metasomatism which produced pure potassic feldspars or alkali feldspar-quartz symplectites. Alteration of plagioclase into albite and potassic alkali feldspar, can be observed within single doleritic plagioclase-clinopyroxene aggregates. The metasomatic fluids transported both sodium and potassium and to a large extent also SiO<sub>2</sub>.

#### Pyroxenes

Pyroxene contents within the Brukkaros sediments are very variable and range from 1-22 vol% in the measured section of the Entrance Valley (Fig. 3). Pyroxenes from the sediments and also from the juvenile lapilli can be

divided into three groups: (I) clear, colourless clinopyroxenes (II) clinopyroxenes partly or completely altered into greenish-brownish aggregates of aegirine, and (III) greenish clear aegirine overgrowths on clear clinopyroxene, calcite, and rounded quartz grains. The rimmed carbonate crystals are apparently pseudomorphs after clinopyroxene. However, rimmed, well rounded calcite also occurs and its origin is highly uncertain.

The pyroxenes are on average between 0.2-0.5 mm, but reach up to 1-2 mm. Smaller pyroxene grains are usually a composite of rounded to angular-subhedral crystals of both fresh type-1 and metasomatically altered type-2 clinopyroxenes. Larger crystals (<0.5 mm) are normally metasomatically altered (type-2) and less rounded. Type-2 pyroxenes also appear in crystal aggregates (or in rock fragments up to a few cm in diameter) together with plagioclase. Clinopyroxene plagioclase aggregates in part show ophitic to intergranular textures resembling textures in the Karoo dolerites.

These relationships between textural maturity and metasomatic alteration (i.e. the proportion of type-2 pyroxenes increases with decreasing roundness and

Code	SNY-Z4-2a	SNY-Z4-2b	43/P3-3b	GB-HMS31	77/P7-12a	GB92-4	73/P2-25b	73/P1-21c	73/P5-27a
Mineral	Cpx	Cpx	Cpx	Cpx	Aegirine	Aegirine	Aegirine	Aegirine	Aegirine
Rock	Sny-	Sny-	GB-	GB-HMS	GB-	GB-	GB-	GB-	GB-
Remark	Dolerite Core	Dolerite Rim	Sediment in lapillus	euhedr.	Sediment alt.Cpx	Dolerite alt.Cpx	Sediment on Cpx	Sediment clear alt. Cpx	Sediment clear
SiO <sub>2</sub>	52.0	50.2	52.2	51.8	51.2	50.9	51.0	50.9	51.2
TiO <sub>2</sub>	0.44	0.74	0.37	0.68	1.41	1.00	5.69	6.03	5.10
Al <sub>2</sub> O <sub>3</sub>	1.66	1.36	2.52	2.24	1.82	0.43	0.19	0.24	0.23
Fe <sub>2</sub> O <sub>3</sub>	0.29	1.05	0.61	0.75	10.1	29.9	25.6	25.8	28.4
Cr <sub>2</sub> O <sub>3</sub>	0.22	<0.02	1.01	0.04	0.04	0.04	0.04	<0.02	0.02
MgO	16.5	13.4	17.1	15.1	7.85	1.35	0.87	0.76	0.91
CaO	17.2	15.5	19.8	18.1	11.7	1.53	0.09	0.06	<0.05
FeO	10.4	15.8	5.93	11.0	8.61	1.27	1.74	1.79	0.59
MnO	0.27	0.34	0.18	0.29	0.24	0.18	0.06	<0.05	<0.05
Na <sub>2</sub> O	0.19	0.16	0.19	0.25	5.24	12.0	13.5	13.6	13.7
K <sub>2</sub> O	<0.03	<0.03	<0.03	<0.03	0.09	0.05	0.03	0.03	0.03
total	99.6	98.6	99.9	100.2	98.3	98.6	98.8	99.1	100.2
Si	1.951	1.938	1.919	1.930	1.968	1.978	1.964	1.954	1.948
Al	0.073	0.062	0.109	0.098	0.082	0.020	0.008	0.011	0.010
Ti	0.012	0.022	0.010	0.019	0.041	0.029	0.165	0.174	0.146
Fe <sup>3+</sup>	0.008	0.031	0.017	0.021	0.294	0.874	0.741	0.745	0.813
Cr	0.006	0.000	0.029	0.001	0.001	0.001	0.001	0.000	0.001
Mg	0.915	0.771	0.934	0.840	0.450	0.078	0.050	0.044	0.052
Fe <sup>2+</sup>	0.325	0.512	0.182	0.343	0.277	0.041	0.056	0.058	0.019
Mn	0.008	0.011	0.006	0.009	0.008	0.006	0.002	0.000	0.000
Ca	0.687	0.642	0.780	0.721	0.483	0.064	0.004	0.002	0.000
Na	0.014	0.012	0.014	0.018	0.391	0.907	1.008	1.011	1.010
K	0.000	0.000	0.000	0.000	0.004	0.002	0.000	0.001	0.001
total	4.000	4.000	4.000	4.000	4.000	4.000	4.000	4.000	4.000
[O]	6.000	6.000	6.000	6.000	6.000	6.000	6.000	6.000	6.000
Akmite	0.20	0.59	0.23	0.43	35.15	91.38	98.50	98.30	98.73
Jadeite	0.57	0.00	0.39	0.57	6.07	0.00	0.00	0.00	0.00
Augite	99.23	99.41	99.38	99.01	58.78	8.62	1.50	1.70	1.27

**Table 4:** Representative pyroxene analyses (augite, aegirineaugite, aegirine) from Gross Brukkaros and the Snyfontein dolerite sill. Fe<sup>3+</sup> calculated from stoichiometry using the method of Droop (1987).

increasing crystal size) suggest a more distally located source for the type-1 clinopyroxenes, compared with the metasomatically altered type-2 crystals. This would be consistent with Gross Brukkaros itself as origin of the metasomatism which altered the source of the type-2 detritus.

Type-3 pyroxenes, the greenish clear, pleochroic aegirine growth-rims, normally measure 5-20  $\mu$  but may reach up to 100  $\mu$ . Aegirine crystallized *in-situ*, after the deposition of the sediments, judging from the growth of aegirine onto rounded and haematite coated quartz grains into the quartz cemented intergranular space (Fig. 7). Further evidence comes from the observation of very fine aegirine needles (length 2-20  $\mu$ , thickness 1  $\mu$ ) and somewhat larger spindle-shaped aegirines (length 20-50

$\mu$ , thickness about 10  $\mu$ ) as inclusions within quartz cement. These aegirine inclusions in quartz are restricted to only a few samples, in which they are very common. There, growth of aegirine and cementation by quartz occurred together and these minerals are syngenetic.

#### Pyroxene Chemistry

Figure 8a shows data points for the Brukkaros pyroxenes and analyses from the Snyfontein dolerite sill plotted in a diagram augite-jadeite-akmite (end member calculations after Banno, 1959). Most of the pyroxenes fall either close to the pure augite or pure akmite end member composition. A few data points plot at intermediate compositions close to the join between these two end members. They come from doleritic pyroxene-

Code	51B/P5	51B/P5	32/P7
Mineral	Mica	Mica	Mica
Remarks	Shale-Pebble	Shale-Pebble	Lapillus
SiO <sub>2</sub>	46.5	46.3	45.8
TiO <sub>2</sub>	1.14	0.59	0.21
Al <sub>2</sub> O <sub>3</sub>	33.5	29.2	30.8
Cr <sub>2</sub> O <sub>3</sub>	0.02	<0.02	<0.02
MgO	1.37	1.74	1.87
CaO	<0.05	<0.05	0.13
FeO	1.18	4.46	2.98
MnO	<0.05	<0.05	<0.05
Na <sub>2</sub> O	0.36	0.29	0.35
K <sub>2</sub> O	10.4	10.7	9.62
total	94.4	93.2	91.7
Si	6.242	6.426	6.368
Al	1.758	1.574	1.632
[4]-Z	8.000	8.000	8.000
Al	3.536	3.200	3.412
Ti	0.115	0.062	0.022
Cr	0.002	0.000	0.000
Mg	0.273	0.359	0.388
Fe <sup>2+</sup>	0.132	0.518	0.347
Mn	0.000	0.000	0.000
[6]-Y	4.058	4.139	4.169
Ca	0.000	0.000	0.020
Na	0.094	0.077	0.094
K	1.784	1.895	1.706
[12]-X	1.888	1.972	1.820
total	13.935	14.111	13.989
[O]	22.000	22.000	22.000
[O]-22 corresponds to [O]-20, [OH, F]-4			

**Table 5:** Representative analyses of muscovites from Gross Brukkaros.

plagioclase aggregates as well as some larger pyroxene crystals, which reflect intermediate stages of the metasomatic alteration.

Figure 8b shows only those pyroxenes with an akmite component of less than 5 mol% in a diagram CaSiO<sub>3</sub>-Mg<sub>2</sub>Si<sub>2</sub>O<sub>6</sub>-Fe<sub>2</sub>Si<sub>2</sub>O<sub>6</sub>. The doleritic pyroxenes from Gross Brukkaros all plot in the Ca- and Mg-rich corner of the augite field towards diopsidic compositions (poldervaart and Hess, 1951). The augites from the Snyfontein dolerite sill partly overlap with the Brukkaros compositions and show an iron enrichment trend which was not found in the detrital pyroxenes at Brukkaros. Also different to the Snyfontein pyroxenes are the high Cr-contents (up to 1.2 wt%) of the Brukkaros pyroxenes with high Mg-numbers (about 80). Such Cr-rich compositions indicate crystallization from quite primitive melts and not compositions like the Snyfontein dolerite sill.

#### Mica

Clear, colourless mica is a very rare ( $\ll 1\%$ ) constituent of the Brukkaros sediments. It is found within clasts

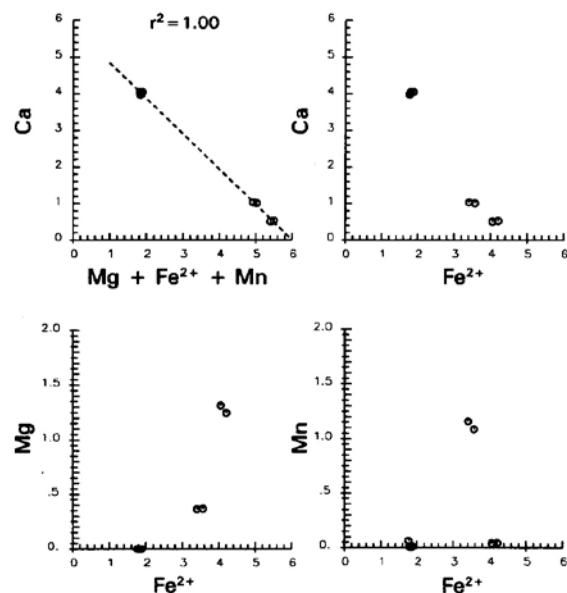
of Nama shales (quartzitic sandy mudstones) or as individual mineral grains, either in the sedimentary matrix or within juvenile lapilli. In size the mica flakes range from 0.1 to 0.3 mm.

Table 5 lists three representative analyses of Brukkaros micas, the first two from Nama shale pebbles, the third from a juvenile lapillus. The sum of the analyses is low and reflects the slightly altered nature of the micas. They are muscovites and not bleached phlogopites. Phlogopites are very common in the surrounding vents and dykes and in the nearby Blue Hills intrusion. The Brukkaros muscovites are derived from mica-bearing shales and sandstones from the Nama Group and/or the Karoo Sequence.

#### Tourmaline

Tourmaline is a very rare ( $\ll 1\text{ vol}\%$ ) mineral of the Brukkaros sediments. It occurs as rounded to subhedral grains, 200-300  $\mu$  in size, within the sedimentary matrix and within the carbonatitic juvenile lapilli, where it is partly resorbed by carbonate.

Table 6 gives two representative microprobe analyses of Brukkaros tourmalines. B, F, and Li were not determined, hence the low totals of the analyses. The tourmaline compositions vary between pure schorl and schorl-dravite solid solutions. Schorl represents the typical granitic/pegmatitic tourmaline, whereas the dravite component might be connected with the Brukkaros metasomatic event. However, other sources for the schorl-dravite solid solutions are also possible.



**Figure 9:** Variations on the A<sup>2+</sup> position of Brukkaros garnets. Plotted are atoms per formula unit on a basis of [O]=24. Figure 9a is a diagram of grossular versus pyrospite and Figure 9b, c, and d indicate the variation of grossular, pyrope and spessartine content with the almandine component.

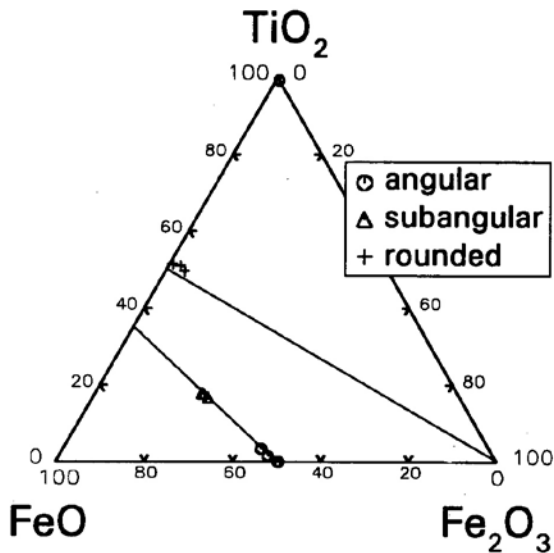


**Figure 10:** Microprobe analyses of oxide phases from Gross Brukkaros sedimentary rocks plotted in a diagram  $TiO_2$ - $FeO$ - $Fe_2O_3$  on mol% basis.

*Garnet*

Rounded garnet grains are extremely rare within the Brukkaros sediments and thus were only observed within the heavy mineral separates gained from the 125-250 $\mu$  sieve class.

Two different types of garnets were observed (Fig. 9 and Tab. 7): (i) almandine-rich garnets with variable pyrope, spessartine, and grossular contents and (ii) grossular-rich garnets with about 1/3 almandine component.

The allmandine- and grossular-rich garnets were probably derived from granitic (the former) or metamorphic (the latter) basement rocks and were possibly transported over great distances prior to deposition within the Brukkaros depocentre. Another possibility would be derivation from basement xenoliths contained in the surrounding pipes and dykes. Pyrope-rich garnets characteristic of kimberlitic source rocks or disintegrated mantle xenoliths were not observed within Brukkaros.

*Oxide Phases*

Apart from the coating around sand grains, haematite is not considered to be a primary detrital component of the Brukkaros sediments, but originated during metasomatic-hydrothermal alteration and diagenesis of the host rock.

Other opaque oxide phases occur mainly as scarce ( $\ll$  1 vol. %) constituents within the juvenile lapilli, but they may also appear within the sedimentary matrix. Lapilli contain a high amount of xenocrystic material so that the oxides within these lapilli may be either detrital or a primary crystallizing phase. The oxides vary in size between 10-200  $\mu$ . They are magnetites to titanomag-

netite solid solutions (with up to about 50 mol% ulvospinel-component), ilmenite, and anatase (Fig. 10, Tab. 8). While magnetite-titanomagnetite and anatase tend to be angular to subhedral, ilmenite grains are anhedral to rounded. This indicates a higher structural maturity of ilmenite grains compared to the other oxide phases. Magnetite and anatase may possibly be derived directly from the carbonatitic volcanic rocks, whereas ilmenite may be derived from Karoo dolerites. The Snyfontein dolerite sill contains mostly magnetite-ilmenite exsolutions and as such it is not a viable source. Other doleritic rocks around Brukkaros are certainly a potential source for the observed Fe-Ti oxide phases.

Rutile, Mg-Al-spinel, Mg-chromites, and magnetite-magnesioferrite solid solutions (Fig. 11) were found in the 125-250  $\mu$  fraction of the heavy mineral samples. Chromites in the Brukkaros sediments suggest contribution of a primary mantle-derived melt, such as kimberlites.

*Carbonate*

Carbonate occurs in various forms within the Brukkaros sediments. Partly rounded calcite, replacing augite, represents the first generation of carbonate formation and might even predate formation of the Brukkaros caldera itself. Haematite stained or coated dolomite rhombohedra (10-100  $\mu$ , average about 50  $\mu$ ) are very common in the sedimentary matrix of some of the Brukkaros rocks. A laminated carbonate layer

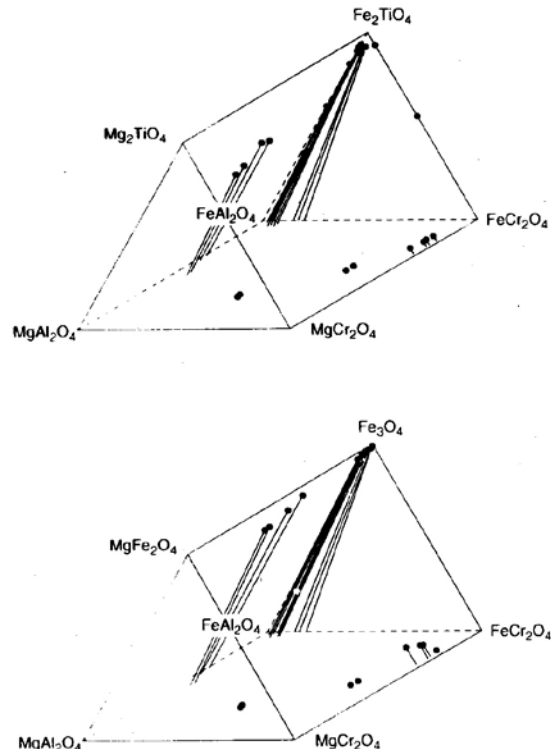


**Figure 11:** Spinel analyses from Brukkaros sedimentary rocks and the 125-250  $\mu$  fraction of Brukkaros heavy mineral samples plotted in the reduced and oxidized spinel prism.

(GB91-32) observed within a sequence of fluvialite sandstones was also shown to consist of dolomite by probe analysis. In this the dolomite crystals show anhedral to subhedral morphologies. Areas with very fine dolomite (about 1  $\mu$ ) vary to zones with better crystallized dolomite (10-50  $\mu$ ), which might represent secondary recrystallization. Calcite appears as colourless rhombohedra with a size between 10-200  $\mu$  (average about 50  $\mu$ ). Both dolomite and calcite rhombohedra were observed as inclusions within later quartz cement or veins. Calcite can also be observed as clear veins or as clear cement. Microprobe analyses showed, however, that within these calcite veins dolomite also occurs. It appears that in calcite quartz veins the crystallization of quartz predates the carbonates. Inclusions of euhedral calcite crystals within quartz veins, however, suggest that multiple events have taken place and in some cases silica veining can follow after calcite growths.

Very fine carbonate (down to about 1  $\mu$ ) also was observed to replace the otherwise turbid matrix of the Brukkaros sediments.

Carbonate analyses are shown in Fig. 12 in a diagram siderite-calcite-magnesite. Calcite and dolomite show some degree of mutual solid solution, and dolomite a solid solution towards ankerite. The three analyses of calcite yielded almost pure  $\text{CaCO}_3$  except for one analysis of colourless, clear cement that contains about 1200 ppm SrO. Dolomite is more variable in its composition and contains up to 2% MnO and 3000 ppm SrO (Fig. 13). The highest FeO content was found in the carbonate rhombohedra and laminated carbonate layer but this may partly stem from haematite staining. The dolomite in the calcite vein ("dykelet", Fig. 13), was free of haematite impurities and contains 2% FeO. The two

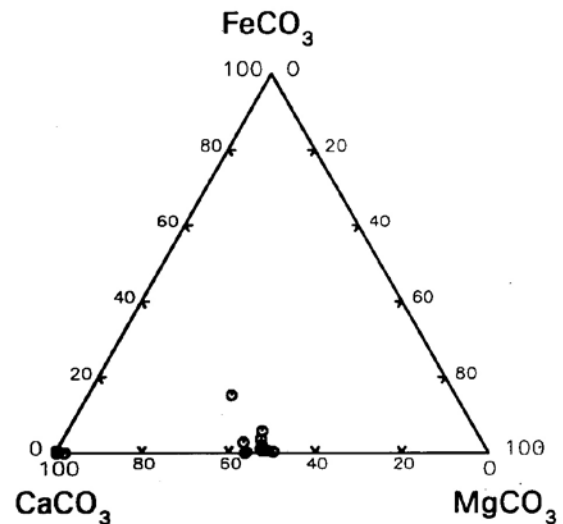


Figure 12: Carbonate analyses from Brukkaros in a diagram  $\text{FeCO}_3\text{-CaCO}_3\text{-MgCO}_3$  (molar proportions)

dolomites with more than 2% MnO are from samples taken from the main river bed for heavy mineral separation. The high Sr contents in almost all carbonates suggest a magmatic origin for the carbonates.

*Sulphates*

*Barite*

In outcrop barite occurs in veins of up to about 1 cm thickness or as euhedral crystals of up to several centimetres in length included in quartz veins. Barite crystallization seems to predate formation of quartz in these veins since barite grows directly from the walls of the veins with no underlying quartz. Thin barite veins, however, may pass laterally into quartz veins on the scale of a thin-section. Replacement of barite by carbonate occurs along the margins of barite veins.

*Gypsum*

Gypsum (Fig. 14) was observed only in very few samples. Where gypsum is very abundant in such samples, it occurs as euhedral, clear parallelogram shaped cross sections (10-50  $\mu$ ) within the quartz cement or grows along the margins of quartz cement and veins. Gypsum and the surrounding quartz are therefore pre- to syngenetic.

*Rock Fragments*

Sand and pebble sized lithic fragments are the main components in the Brukkaros sandstones and conglomerates. They include the previously mentioned doleritic crystal aggregates and pebbles and mainly silicified shales and cherts. Chert here refers to fragments where the shale matrix is almost completely replaced by very fine quartz (2-20  $\mu$ ). This clay-silt replacement by quartz might be related to the metasomatic-hydro-

Mineral	Schorl	Schorl-Dravite
Code	45/P10	0.4A/20°
Shape	Round	Subhedral
SiO <sub>2</sub>	34.5	36.2
TiO <sub>2</sub>	<0.04	0.52
Al <sub>2</sub> O <sub>3</sub>	33.6	30.8
Cr <sub>2</sub> O <sub>3</sub>	<0.02	0.03
MgO	0.17	7.24
CaO	0.24	0.39
FeO	14.9	7.59
MnO	0.26	<0.05
Na <sub>2</sub> O	1.96	2.26
K <sub>2</sub> O	0.06	<0.03
<b>total</b>	<b>85.7</b>	<b>85.0</b>

Table 6: Tourmaline compositions from the Brukkaros sediments.

Code	0.2A/20° Z2-1	0.2A/20° Z2-3B	0.4A/20° Z1-5	0.2A/20° Z2-4	0.2A/20° Z2-6
SiO <sub>2</sub>	37.1	36.5	37.3	37.4	37.8
TiO <sub>2</sub>	0.06	0.07	0.05	0.06	< 0.04
Al <sub>2</sub> O <sub>3</sub>	20.4	20.6	21.2	23.3	22.1
Cr <sub>2</sub> O <sub>3</sub>	0.03	0.05	< 0.02	< 0.02	< 0.02
Fe <sub>2</sub> O <sub>3</sub>	0.30	1.07	1.65	0.00	0.25
MgO	1.52	1.50	5.56	< 0.05	< 0.05
CaO	5.78	5.90	3.00	23.7	24.0
FeO	26.3	25.0	30.6	13.5	14.3
MnO	7.89	8.39	0.30	0.48	0.07
total	99.3	99.1	99.7	98.4	98.6
Si	6.022	5.951	5.913	5.859	5.934
Al [4]		0.049	0.087	0.141	0.066
Z	6.022	6.000	6.000	6.000	6.000
Al [6]	3.900	3.895	3.880	4.162	4.036
Ti	0.008	0.008	0.005	0.007	0.000
Cr	0.004	0.007	0.000	0.000	0.000
Fe <sup>3+</sup>	0.037	0.131	0.196	0.000	0.030
B	3.949	4.041	4.081	4.169	4.066
Mg	0.369	0.364	1.313	0.000	0.000
Ca	1.007	1.030	0.510	3.976	4.047
Fe <sup>2+</sup>	3.568	3.407	4.055	1.772	1.878
Mn	1.085	1.158	0.041	0.063	0.010
A	6.029	5.959	5.919	5.811	5.935
total	16.000	16.000	16.000	15.981	16.000
[O]	24.000	24.000	24.000	24.000	24.000

**Table 7:** Microprobe analyses of garnets from Gross Brukkaros. Fe<sup>3+</sup> calculated from stoichiometry after Droop (1987).

thermal alteration of wall rocks caused by the intrusion of the Brukkaros magma reservoir. The shales and cherts can contain muscovite (10-100 μ) or very fine quartz sand of low maturity (often subangular). Within the silicified or cherty matrix carbonate patches (50-100 μ) sometimes occur, documenting secondary quartz replacement, and secondary crystallization of carbonate rhombohedra (about 50 μ in diameter) is also observed. Within cherts, haematite can form needles about 1-10 μ long, which sometimes form clusters of 100-200 μ in diameter causing a dotted appearance of the rock fragments. A few cherty shale fragments contain isolated rounded quartz sand grains and are interpreted in terms of silicified glaciomarine sediments of the Dwyka Formation. A Dwyka Formation origin is also probable for some fine to very fine grained sandstone fragments with a cherty silt matrix-supported fabric.

Fragments of quartzitic sandstone are possibly derived from the Haribes Member quartzites (Nama Group) but are extremely rare. They consist of fine sandstone with varying proportions of cherty matrix. Thus Nama quartzites were not available as source rocks at the syn-Brukkaros erosional surface.

Scarce opaque sand grains and pebbles, which can in-

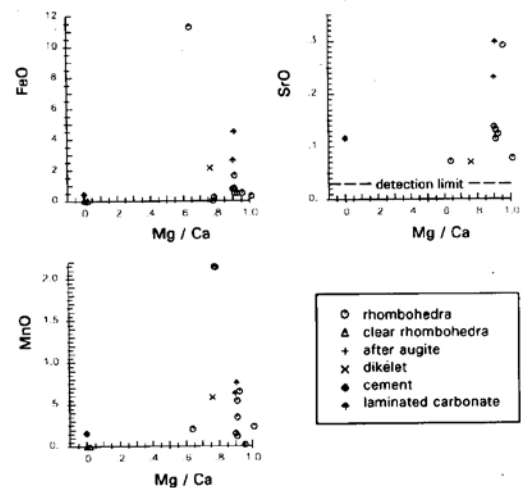


**Figure 13:** FeO and trace elements in carbonates from Gross Brukkaros.

clude some very fine quartz, consist of pure haematite and are interpreted as lateritic concretions.

The interpretation of clasts with a poikilotopic fabric is uncertain. Here, quartz and shale sand grains, augite, augite replaced by aegirine or with aegirine overgrowth, plagioclase, and carbonate are enclosed by secondary crystallized quartz (crystal size commonly 0.05-0.1 mm). We interpret these clasts as reworked quartz veins from Gross Brukkaros because of the occurrence of aegirine alteration and overgrowth. These fragments demonstrate that the metasomatic and hydrothermal alteration of the Brukkaros sediments was not only a postdepositional but also a syn-depositional event.

Further evidence for such an interpretation comes from one sample where the coarser quartz sand grains (average size about 0.35 mm) actually are monomineralic rock fragments. The quartz crystals show neither sutured grain boundaries nor triple point equilibrium textures and an origin from reworked hydrothermal quartz veins appears to be very likely. Carbonate inclusions occur in some of these quartz grains similar to those common within quartz veins and cements from the Brukkaros sediments.

The grain size of the dominant shale and chert fragments is very variable and may exceed pebble-size (up to 20 cm). Lithic fragments in thin-sections of the sandstones and gravelly sandstones range between 0.06 and 5 mm (i.e. very fine sand to pebble size). In some samples a negative correlation between grain size and structural maturity can be observed: the coarser (> 1 mm) shale and chert fragments commonly are angular to sub-angular with low sphericity (i.e. platy shapes), while the opposite can be found, however, in other samples. The finer grains are mostly rounded with an intermediate sphericity (elliptical grain morphology), angular to subangular platy fragments, however, are

also common.

The presence of well rounded, spherical lithic sand grains indicates input of previously aeolian transported material. Additional evidence for arid or at least semi-arid conditions comes from the observation that all smaller lithic fragments are coated by haematite (10-1  $\mu$ , commonly <5  $\mu$ , Fig. 15). In the coarser fragments some grains show haematite coating whereas others appear to be free of it.

*Fragmented Magmatic Carbonatite, Juvenile Carbonatite Lapilli*

*Magmatic carbonatite*

In the field very rare pebble to cobble-sized fragments of magmatic carbonatite can be observed within the Brukkaros sediments. Due to the absence of phenocrysts in these very fine grained and altered magmatic clasts they cannot be distinguished from oxidized mudstone fragments in thin section. Macroscopically, however, the carbonatite fragments can be recognized by the lack of bedding characteristics as well as the presence of pebble-sized lithic inclusions. The angular shape of these clasts indicates fragmentation of solidified rocks, either during explosive pipe formation (fragmentation of precursor dykes) or during sedimentary processes.

*Juvenile lapilli*

The content of juvenile lapilli is very variable in the Brukkaros sediments. If present at all, the modal

proportions in the fluvialite, debris flow, and mudflow deposits range between about 2-20%. A few individual beds observed at the western rim of Gross Brukkaros include up to 70 vol% of juvenile lapilli, thus showing a lapilli supported fabric. The lack of bedding as well as the poor sorting (unless the sandy matrix infiltrated after deposition) indicate redeposition and not primary deposition from airfall processes.

All carbonatitic lapilli are characterized by a high proportion of xenocrystic material (Fig.16). From the appearance of their matrix, however, three types of juvenile lapilli may be distinguished: (i) lapilli with a matrix of fine (about 5  $\mu$ ), anhedral, colourless carbonate, (ii) similar lapilli with a dark grey coloured matrix, and (iii) lapilli with an unidentifiable reddish-brown, buff coloured or almost opaque, haematite and limonite stained matrix, which appears to be carbonate-rich as well.

The first type was only observed at the western to northwestern rim of the Brukkaros crater. Greenish-grey fragments of the second type are quite common within several samples from the Brukkaros sediments. Within the lowermost metres of the Brukkaros sediments towards the contact with the underlying Nama or Karoo beds these greenish lapilli can become increasingly replaced by secondary clear quartz. The brownish type-3 lapilli are the most common type within the Brukkaros sediments, but may be difficult to distinguish from re-worked Brukkaros material occasionally.

The first two lapilli types commonly have rims of

Code	45/P8-4	77/P1-6a	51B/P7-7a	HMS-1a	HMS-1b	HMS-13a	HMS-14a	HMS-15a	HMS-15b	Sny4a	45/P7-3a	45/P7-3b	HMS-10	SNY-3a	SNY-4c	45/P2-5b	HMS-19
Mineral	Spinel										Ilmenite					Anatase	Rutile
SiO <sub>2</sub>	<0.05	0.19	<0.05	0.07	0.07	0.09	<0.05	<0.05	<0.05	<0.05	<0.05	0.19	<0.05	0.09	0.09	0.36	<0.05
TiO <sub>2</sub>	<0.04	1.03	13.6	11.8	10.9	1.33	2.23	0.08	0.05	16.7	50.3	52.1	44.0	51.4	50.2	95.7	98.8
Al <sub>2</sub> O <sub>3</sub>	<0.05	0.46	0.43	5.30	5.55	8.67	1.07	29.5	29.1	1.50	<0.05	<0.05	<0.05	<0.05	<0.05	<0.05	<0.05
Fe <sub>2</sub> O <sub>3</sub>	68.5	85.3	42.1	45.3	47.1	0.00	7.10	0.76	1.11	34.7	4.99	1.19	15.5	2.96	4.36	1.28	0.11
Cr <sub>2</sub> O <sub>3</sub>	<0.02	0.02	0.05	0.54	0.59	60.0	58.1	41.3	41.4	0.13	0.05	0.04	0.03	0.02	0.02	0.17	0.19
MgO	<0.05	<0.05	0.89	11.75	12.2	9.17	6.18	15.9	15.8	0.07	1.90	1.58	<0.05	0.81	0.26	<0.05	<0.05
CaO	0.25	<0.04	<0.04	0.11	0.09	<0.04	<0.04	<0.04	<0.04	0.05	<0.04	<0.04	<0.04	0.10	0.12	1.32	<0.04
FeO	30.4	32.0	41.8	23.7	22.3	19.3	23.5	11.9	11.7	45.7	41.3	43.8	39.4	44.3	44.3	0.00	0.00
MnO	<0.05	<0.05	0.20	0.89	0.92	0.50	0.71	0.35	0.34	0.83	0.48	0.41	0.11	0.43	0.36	<0.05	<0.05
NiO	0.08	<0.05	<0.05	<0.05	<0.05	0.05	0.21	0.10	0.11	<0.05	<0.05	<0.05	<0.05	<0.05	<0.05	<0.05	.
ZnO	<0.05	<0.05	<0.05	0.09	<0.05	0.12	<0.05	0.11	0.14	.	<0.05	0.06	.	.	.	0.05	.
total	99.2	99.1	99.0	99.6	99.7	99.2	99.1	99.9	99.9	99.8	99.0	99.3	99.1	100.0	99.7	98.9	99.1
Si	0.000	0.007	0.000	0.002	0.002	0.003	0.000	0.000	0.000	0.000	0.000	0.005	0.000	0.002	0.002	0.005	0.000
Ti	0.000	0.030	0.388	0.303	0.278	0.034	0.060	0.002	0.001	0.473	0.952	0.984	0.850	0.970	0.956	0.974	0.998
Al	0.000	0.021	0.019	0.213	0.222	0.344	0.045	1.020	1.009	0.067	0.000	0.000	0.000	0.000	0.000	0.000	0.000
Fe <sup>3+</sup>	2.000	1.904	1.204	1.161	1.201	0.000	0.191	0.017	0.025	0.984	0.095	0.022	0.300	0.056	0.083	0.013	0.001
Cr	0.000	0.001	0.002	0.014	0.016	1.595	1.644	0.959	0.964	0.004	0.001	0.001	0.001	0.000	0.000	0.002	0.002
Mg	0.000	0.000	0.050	0.597	0.618	0.459	0.330	0.696	0.695	0.004	0.071	0.059	0.000	0.030	0.010	0.000	0.000
Ca	0.010	0.000	0.000	0.004	0.003	0.000	0.000	0.000	0.000	0.002	0.000	0.000	0.000	0.003	0.003	0.019	0.000
Fe <sup>2+</sup>	0.988	-1.037	1.331	0.677	0.633	0.541	0.703	0.293	0.292	1.440	0.871	0.919	0.847	0.930	0.937	0.000	0.000
Mn	0.000	0.000	0.006	0.026	0.026	0.014	0.022	0.009	0.009	0.026	0.010	0.009	0.002	0.009	0.008	0.000	0.000
Ni	0.002	0.000	0.000	0.000	0.000	0.001	0.006	0.002	0.003	0.000	0.000	0.000	0.000	0.000	0.000	0.000	.
Zn	0.000	0.000	0.000	0.002	0.000	0.003	0.000	0.002	0.003	.	0.000	0.001	.	.	.	0.000	.
total	3.000	3.000	3.000	3.000	3.000	2.994	3.000	3.000	3.000	3.000	2.000	2.000	2.000	2.000	2.000	1.014	1.001
(O)	4.000	4.000	4.000	4.000	4.000	4.000	4.000	4.000	4.000	4.000	3.000	3.000	3.000	3.000	3.000	2.000	2.000

**Table 8:** Microprobe analyses of primary magmatic oxide phases observed at Gross Brukkaros (whole rock and heavy mineral samples ("HMS") and the Snyfontein dolerite sill ("Sny"). Fe<sup>3+</sup> calculated from stoichiometry after Droop (1987).

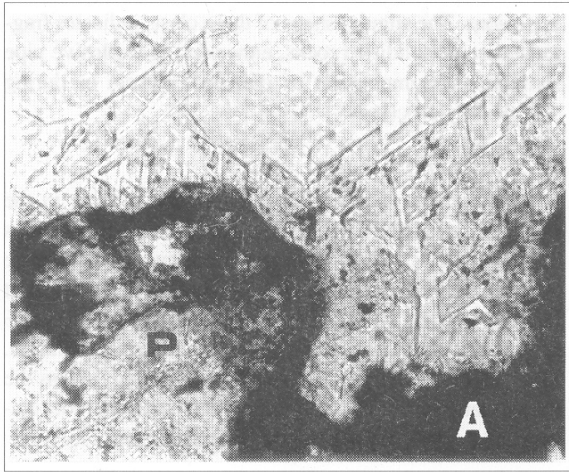


**Figure 14:** Euhedral gypsum crystals (10-50  $\mu$ ) intergrown with clear quartz cement on altered plagioclase (P) and augite (A). Sample GB91-47, E side crater floor, coarse grained, fluvatile sandstone, picture width: about 0.2 mm.

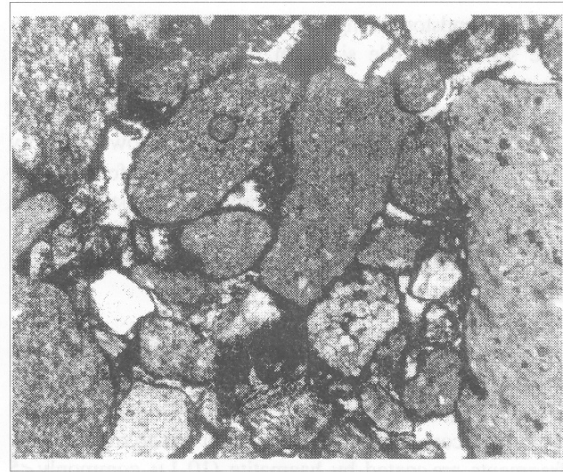


**Figure 15:** Rounded to angular shale sand grains coated by haematite. The rock is cemented by clear quartz. Sample GB91-77, fluvatile sandstone, Entrance Valley, profile layer P2 (Fig.3), picture width: about 1.5 mm.

palisade shaped, recrystallized carbonate around crystalline inclusions (Fig. 17). These rims are absent or relatively thin near the margins of the lapilli, but increase in thickness (10-100  $\mu$ ) towards the centre. Crystalline inclusions commonly show marginal resorption by carbonate.

In one lapilli bed on the western crater-rim, coating of the lapilli by slightly darker coloured, laminated carbonatic material was observed. It remains uncertain whether this represents a magmatic accretion processes (autolith growth) or some kind of post-depositional concretion.

Aegirine overgrowth, mainly on augite, is also quite common. If coated by a rim of recrystallized carbonate this aegirine overgrowth is also partly resorbed. Crystalline inclusions on average form about 20-30 vol% of the lapilli of both types (Tab. 9). Quartz, augite and feldspar (in descending order) are the main inclusions, all of which can become partly or completely replaced by carbonate. Scarce oxide phases and, even more rarely, tourmaline also occur.

Rounded to euhedral inclusions (100-500  $\mu$ ) occur very rarely in the buff coloured lapilli. They are now completely replaced by iron-oxide, iron-hydroxide, and carbonate. The euhedral shapes resemble the outlines of small olivine phenocrysts. However, they may also be pseudomorphs after pyroxene, since in these lapilli only unusually few, strongly altered augite crystals occur.

Lithic fragments are commonly components ( $\leq 1\%$ ) of the lapilli. They include dolerite, cherty shale, fine sandstone, and quartzite. Shale fragments are largely replaced by carbonate.

#### *Composition of juvenile lapilli*

The division of the juvenile lapilli according to their optical appearance (clear/greenish/brownish) also holds

in the chemical characterization (Fig. 18 and Tab. 10) in that (i) the clear lapilli are calcitic carbonatites, (ii) the greenish ones are aegirine-bearing, calcitic lapilli with siderite solid solution, and (iii) the brownish ones are dolomitic lapilli. Since the brownish type-3 lapilli are commonly very hard to distinguish from reworked Brukkaros material, only three analyses are reported (samples GB91-34 and -51), which faithfully represent juvenile material.

Carbonate within the clear lapilli must be calcite which may host some of the iron ( $\text{FeO}_{\text{total}}$  0.2-4 wt%) as sideritic solid solution component.  $\text{SiO}_2$  contents range from  $<1$  to 36 wt% (Tab. 10) which probably reflects diagenetic silicification rather than primary differences in magma composition.

The comparatively high  $\text{SiO}_2$  contents (30-43 wt%, with only lapilli containing no obvious  $\text{SiO}_2$  replacement features used for analyses) and sums of analysis (79-87 wt%) of the greenish-grey lapilli indicate that carbonate is not the only major matrix constituent. CaO (23-6 wt%) and FeO (23-13 wt%) appear to be negatively correlated and haematite staining is absent. This suggests the presence of Ca-Fe carbonates. The high  $\text{Nb}_2\text{O}_5$  (1600-2300 ppm) and  $\text{TiO}_2$  (about 2 wt%) contents and especially the very high sodium contents ( $\text{Na}_2\text{O} = 7-11\text{ wt}\%$ ) suggest alteration of the greenish lapilli by metasomatic processes. The chemical features and the greenish colour indicate the presence of aegirine in the matrix. Grain sizes of the matrix are too small to be resolved with the optical microscope so that aegirine cannot be identified with confidence in the matrix. It is however, present in identifiable sizes as thin rims around mineral inclusions. The greenish grey lapilli may thus be products of polyphase alteration of the "normal" carbonatite lapilli described above. This alteration would include (predepositional) metasomatic

introduction of Na, Nb, Ti, and Fe and a second post-depositional silicification event.

One averaged analysis (GB91-34, P9) of a brownish to opaque lapillus has extremely high  $P_2O_5$  (9 wt%) at relatively high  $SiO_2$  (27 wt%) and high SrO (1200 ppm). It is not included in Fig.18. The other two averaged lapilli compositions can be distinguished from type-1 by high MgO (about 16 wt%) and MnO contents (1 and 0.6 wt%) and low  $SiO_2$  (< 4 wt%) at a given  $P_2O_5$  (about 0.6 wt%) content (Fig. 18). Low  $Na_2O$  (about 1000 ppm) and  $Nb_2O_5$  contents (< 0.04 wt%) make a metasomatic alteration of these lapilli unlikely. Thus, a second magma type of primary magnesio-carbonatitic composition is documented by these lapilli.

Comparison of minor and trace elements of type-1 (calciocarbonatites) and type-3 (dolomitic) lapilli with average calciocarbonatites (Tab. 10 and Fig. 19) and magnesio-carbonatites given by Woolley and Kempe (1989) and with averaged alvikite dykes from Katz and

Keller (Tab. 10, from Keller *et al.*, 1990) shows the following: Cr and partly Ti are somewhat higher than in the literature data.  $P_2O_5$  contents lie somewhat below these averages but within the reported range of values (Woolley and Kempe, 1989). Mn contents are similar to the magnesio-carbonatites in the type-3 lapilli but are low in the type-1 lapilli compared to the calciocarbonatites. The observed Nb contents are mostly at or below the detection limit of <0.04 wt% and thus low compared to the average values reported by Woolley and Kempe (1989), which however, are highly variable. BaO, reported only for lapilli with  $TiO_2$  below detection limit because of peak overlap, is well below the reported average values. So is SrO, which is roughly 10 times lower on average and similar to the <400-1400 ppm of the matrix of the host sediment. These are geochemical features unusual for "normal" carbonatites but similar to a large number of carbonatite dykes and necks in the surroundings of Gross Brukkaros (Kurszlaukis, *in prep.*).

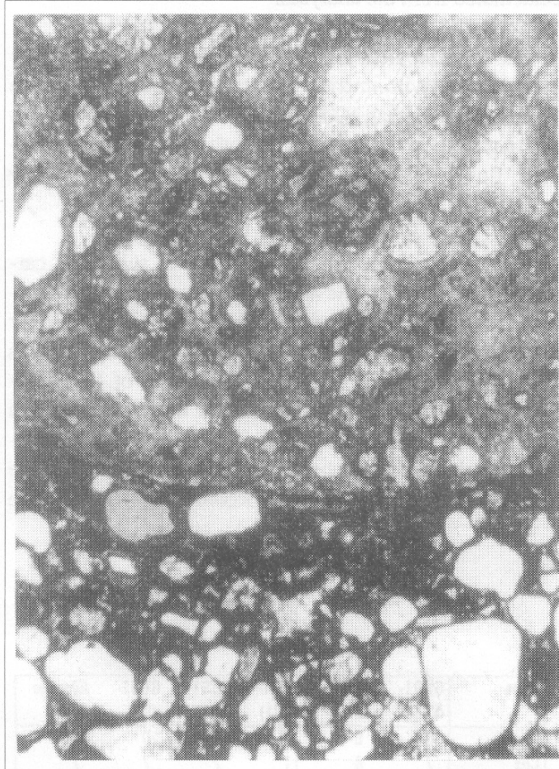


**Figure 16:** Calciocarbonatitic lapillus (top), rich in xenocrystalline inclusions of quartz and augite. The lapillus is embedded in a sediment consisting of rounded to subrounded quartz grains with a haematite stained, carbonate-rich matrix. Sample GB91-VL1, Wrim Brukkaros, picture width: about 2.5 mm

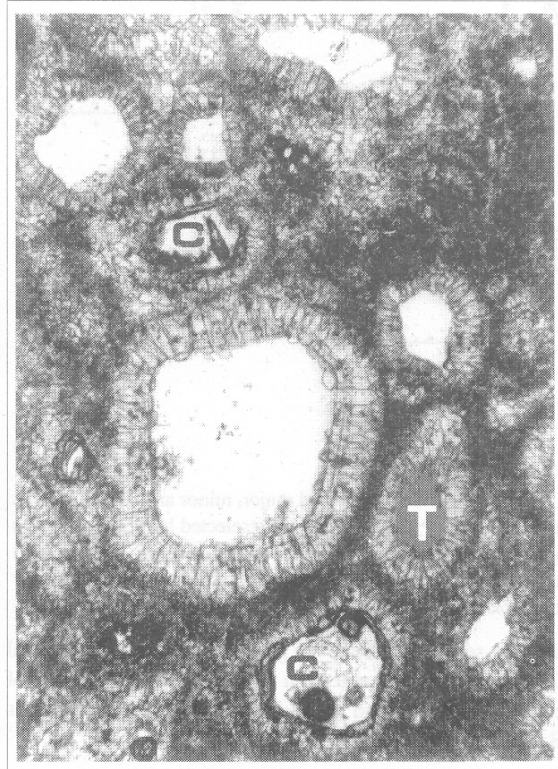


**Figure 17:** Xenocrysts in a calciocarbonatitic lapillus. The inclusions show well developed rims of palisade shaped calcite. The palisade rim around the quartz grain in the centre of the picture shows a concentric pattern. This is interpreted in terms of neomorphic replacement of a pre-existing concentric fabric in the carbonatitic lapilli matrix. The quartz grain itself shows marginal resorption by calcite. Two calcite inclusions (C), probably pseudomorphs after augite, are rimmed by aegirine. The aegirine again is rimmed and partly resorbed by palisade calcite. The grey inclusion (T) is a greenish, strongly resorbed tourmaline (0.15 mm). Sample: GB91-45, NW-rim of Brukkaros, picture width: about 1 mm.

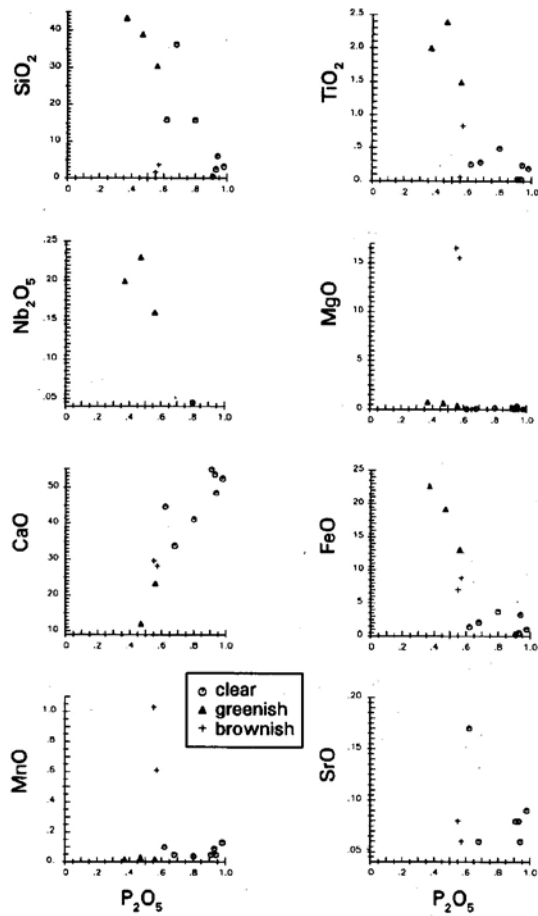


**Figure 18:** Some selected major, minor and trace elements plotted versus P<sub>2</sub>O<sub>5</sub>. Phosphorus is selected because it shows a good negative correlation with SiO<sub>2</sub> (except for the brownish type-3 lapilli), and thus seems to be an indicator for primary compositions.

*Matrix / Cement*

The lithic and mineral grains and pebbles of the Brukkaros sandstones and conglomerates sit in a turbid intergranular matrix and/or are cemented in various ways.

The brownish, haematite stained matrix is too fine grained for the identification of individual crystals with the optical microscope. Nevertheless, matrix areas with little haematite staining show in most cases high birefringence thus indicating carbonate. These samples also show distinct reaction with HCl.

The matrix has a low birefringence in some other samples, which is the case in all samples from the red sandy mudstone cropping out in the upper part of the major “Entrance Valley”. There SiO<sub>2</sub> forms a major part of the muddy matrix.

Janse (1969) reports results from X-ray diffractometry of the matrix of the Brukkaros “microbreccias”, which show mostly feldspar (presumably present as very fine-grained dust) and subordinate quartz, calcite, and dolo-

mite as essential constituents. Janse (1969) assumed K-feldspar as the major matrix constituent because of the high potassium content of these samples. Microprobe analyses of the turbid matrix do not, however, support this assumption because only one of thirteen analyses contained enough K (Tab. 11, analysis 68, K <2 wt%, K >Na) to allow for the possibility of potassium dominated alkali feldspar (see Tab. 11). Otherwise the turbid matrix consists either of carbonate (dolomite or calcite) and oxide minerals (± excess silica) or of albite plus oxide phases ± carbonate and excess silica as may be recalculated from the analyses.

The trace element contents of the matrix reflect partly the volcanic environment with high (for sediments) Sr<sub>2</sub>O<sub>3</sub> contents of more than 1000 ppm which may be attributed to leaching from juvenile lapilli and ash grains or to metasomatic fluids emanating from a magma chamber below Brukkaros.

Colourless, inclusion-rich, anhedral to subhedral carbonate patches within the haematite stained carbonatic matrix are common. These patches can be mono- (20-60 μ) or poly-crystalline (up to 0.5 mm). Such crystals and patches can also be found in the silica-rich matrix of the sandy mudstones. These carbonates are due to recrystallization which transforms the rock matrix into a mosaic of polycrystalline carbonate with haematite displaced towards the boundary between individual carbonate aggregates. The aggregates have an average size of about 50 μ, the individual anhedral carbonate crystals range from 5 μ to 50 μ.

Cementation by colourless, clear carbonate also occurs, which concurs with the displacement of quartz and quartz grains even if haematite coated. Resorbed quartz was observed as relicts located in the centre of carbonate veins and cement patches. Carbonate cementation can be accompanied by barite cementation.

However, cementation by quartz exceeds by far the cementation by clear carbonate and is commonly, but not invariably associated with haematite stained carbonate-rich matrix. Grain sizes in the quartz cement

Code	GB91-43 (1)	GB91-43 (2)	GB91-44 (1)	GB91-44 (3)	GB91-VL1	Average
Quartz	8	6	10	18	10	10
Cpx	7	8	11	2	7	7
Oxides	0.3	0.3	0	0	0	0.1
Plagioclase	5	5	7	7	4	6
Microcline	0.3	0.5	0.4	0.3	1.1	0.5
Shale	0	0	2	0	0.5	0.5
Matrix	81	80	70	73	77	76

**Table 9:** Modal proportions of xenocrystic mineral and lithic inclusions within juvenile lapilli from Gross Brukkaros. Between 500 and 1000 points were counted on lapilli ranging in diameter between about 5-10 mm. GB91-43 represents greenish-grey type-2 lapilli, whereas the other two samples contained clear type-1 lapilli.

range from 50  $\mu$  to 100  $\mu$ . If however, quartz cement actually forms as a rim cement on sand grains (with the same crystallographic orientation) it may become quite coarse grained (up to about 0.5 mm). Quartz veins vary between about 0.1 mm to several centimetres in size. Quartz cement and veins have in part poikilotopic textures. From growth relationships, or their appearance as fine euhedral inclusions within quartz cement, a partly syngenetic relationship can be deduced with calcite, barite, gypsum and aegirine crystallization.

**Discussion and conclusions**

To summarize, the mineral and lithic constituents of the Brukkaros sediments can be divided into six main groups.

**I. Shales and cherts derived from the Karoo Sequence and the Nama Group:**

Sediments of the Karoo Sequence in outliers preserved as inselbergs 5 km east of Brukkaros and of Dwyka Formation (lowermost Karoo) as wall rock of the Brukkaros sediments themselves (Stachel *et al.*, 1994) prove the presence of a Karoo cover on top of the Nama rocks at least as far west as Brukkaros during the Upper Cretaceous. Clasts of the Nama group quartzites (Haribes Member) are practically absent, which indicates that incision into the local stratigraphy did not go deeper than Nama Group shales of the Rosenhof Member. These shales are exposed on the inner slopes of the caldera. These observations are consistent with the structural reconstruction of the caldera evolution (Stachel *et al.*, 1994).

Thus, the Dwyka and Prince Albert Formations of the Karoo Sequence form the prime source for the sand-, pebble-, and cobble-sized shale fragments within the

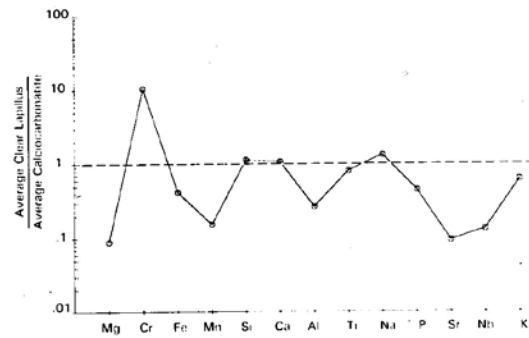


**Figure 19:** Spider diagram for clear lapilli using a normalization to the average calcite-carbonatite composition of Woolley and Kempe (1989). For the calculation of the average for the clear lapilli only four lapilli with SiO<sub>2</sub> 1 < 10 wt% were used.

Brukkaros sediments, but pebbles and cobbles of red-coloured shale and bleached shale with red cores might be identified as Nama shales as well.

The muddy matrix of the Brukkaros sediments is attributed to the same sources.

**II. Monocrystalline quartz grains of probable aeolian origin:**

Quartz grains at Brukkaros are generally monocrystalline. Therefore, they cannot have been derived by disaggregation of quartzites, because in this case all types should be preserved from mono- to polycrystalline examples. Thus the grains must have been derived from an unconsolidated or poorly consolidated source. Possible candidates include Karoo sandstones and younger Mesozoic sediments.

About 10-20% of the quartz grains have very high

Code	44/P9	44/P10	GB91- VL1/P2	45/P11	45/P14	GB91- VL1/P1	45/P5	43/P1	43/P3	43/P4	51B/P8	34/P3	34/P9	Katz & Keller	Woolley & Kempe	Taylor & McLennan
Remarks	clear							greenish			brownish			Alvikite	C-carb.	Shale
P <sub>2</sub> O <sub>5</sub>	0.93	0.91	0.98	0.94	0.80	0.62	0.68	0.56	0.47	0.37	0.55	0.57	9.01	1.74	2.10	0.16
Nb <sub>2</sub> O <sub>5</sub>	<0.04	<0.04	<0.04	<0.04	0.04	<0.04	<0.04	0.16	0.23	0.20	<0.04	<0.04	<0.04	0.12	0.17	0.002
SiO <sub>2</sub>	2.46	0.52	3.20	6.04	15.8	15.9	36.3	30.4	39.0	43.4	1.67	3.66	27.5	1.69	2.72	62.8
TiO <sub>2</sub>	<0.04	<0.04	0.19	0.24	0.49	0.25	0.28	1.49	2.39	2.00	0.06	0.83	1.36	0.09	0.15	1.00
Al <sub>2</sub> O <sub>3</sub>	0.14	0.02	0.38	0.59	2.58	1.04	0.38	2.06	0.46	0.41	0.33	0.41	1.29	0.48	1.06	18.9
Cr <sub>2</sub> O <sub>3</sub>	<0.03	0.03	<0.03	0.04	0.04	<0.03	<0.03	<0.03	0.03	0.04	<0.03	<0.03	0.04		0.002	0.016
MgO	0.10	0.15	0.05	0.34	0.17	0.06	0.10	0.42	0.66	0.77	16.5	15.5	3.10	0.73	1.80	2.20
CaO	53.5	55.0	52.4	48.4	41.1	44.6	33.7	23.3	12.1	5.72	29.6	28.2	17.4	49.0	49.1	1.30
FeO	0.48	0.24	1.08	3.27	3.73	1.39	2.09	13.1	19.2	22.7	7.06	8.82	11.8	2.73	3.03	6.50
MnO	0.09	0.05	0.13	0.05	<0.05	0.10	0.05	<0.05	<0.05	<0.05	1.03	0.61	0.16	0.69	0.52	0.11
ZnO	0.07	<0.06	<0.06	<0.06	<0.06	0.06	<0.06	<0.06	<0.06	<0.06	<0.06	<0.06	<0.06		0.02	0.01
SrO	0.08	0.08	0.09	0.06		0.17	0.06	<0.04	<0.04	<0.04	0.08	0.06	0.12	0.93	0.86	0.024
BaO	<0.06	<0.06												0.20	0.34	0.073
Na <sub>2</sub> O	0.20	0.10	0.59	0.63	2.64	0.77	1.05	6.50	9.57	11.1	0.12	0.10	0.30	0.08	0.29	1.20
K <sub>2</sub> O	0.05	<0.03	0.24	0.36	0.84	0.92	0.22	1.21	0.29	0.15	0.07	0.05	0.07	0.09	0.26	3.70
total	58.2	57.1	59.3	61.1	68.4	66.0	75.0	79.2	84.4	86.8	57.2	58.9	72.2	58.6	62.4	98.0

**Table 10:** Chemical composition of lapilli included into the Brukkaros sedimentary sequence. Each reported composition represents the average of four analyses of crystal-inclusion free matrix areas of 10-20  $\mu$  diameter. Ba is only reported for Ti-free analysis, because of interferences.

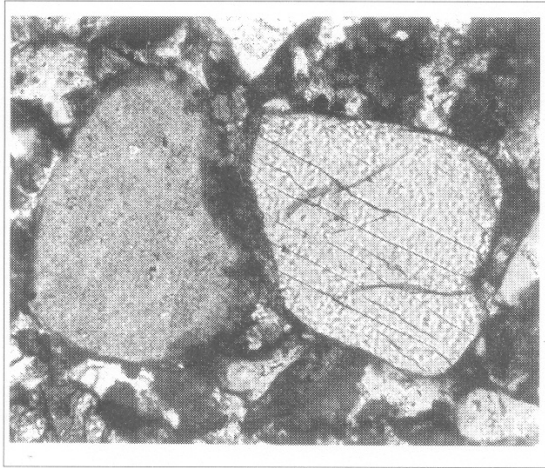


**Figure 20:** Completely fresh, subrounded grain of augite (0.25 mm), rimmed by haematite. Rounded grain of chert (0.25 mm) to the left. Sample: GB91-43, WSW-rim of Brukkaros, picture width: about 0.5 mm.

textural maturity, showing well rounded and highly spherical shapes (Fig. 5) and a grain size variation restricted to two “Phi” intervals. These characteristics are suggestive of an aeolian environment as a source, which is supported by the haematite coating described. The simplest explanation is that the Kalahari basin sediments were already extant at the time of the genesis of Gross Brukkaros (Upper Cretaceous).

### III. Dolerite fragments and doleritic mineral grains:

Karoo dolerites contributed as lithic fragments and as mineral grains to the fill of the Brukkaros depocentre. Some beds of the Brukkaros sequence consist of more than 50% of doleritic material. This indicates an intrusive source, probably sills, very close to Gross Brukkaros, but which is completely eroded today. A second source of intrusive material was situated at somewhat greater distance and this provided the texturally more mature and metasomatically unaltered grains. Augite (Fig. 20) and relatively basic plagioclase grains survived the disaggregation of their host rock without total alteration which indicates rapid mechanical weathering which avoided chemical weathering. This is in accord with aeolian transported sand grains (see above). Inferences on climate at the time of the formation of Gross Brukkaros can be drawn from these observations. Karoo dolerites may also be the main source for the rare detrital oxide minerals within the Brukkaros sediments.

### IV. Crystal fragments of basement rocks:

Microcline, tourmaline, and grossular-rich garnet are primarily attributed to basement rocks. They are probably derived from disaggregated basement xenoliths from the surrounding diatremes (Rupprecht, *in prep.*). Tourmaline, garnet, as well as some of the detrital oxide grains may, however, also have stemmed from the

Sample	GB91-1	GB91-1	GB91-1	GB91-1	GB91-1	GB91-4	GB91-1	GB91-4	GB91-1
Code	57	VL1 70	VL1 67	VL1 68	58	73	1P6 55	74	56
P <sub>2</sub> O <sub>5</sub>	0.49	0.93	0.52	0.94	0.29	0.37	0.27	0.27	<0.05
Nb <sub>2</sub> O <sub>5</sub>	<0.04	<0.04	<0.04	<0.04	0.11	<0.04	0.30	<0.04	<0.04
SiO <sub>2</sub>	0.20	2.94	13.0	15.3	23.9	33.4	50.4	54.0	71.6
TiO <sub>2</sub>	<0.04	0.04	0.81	0.55	1.11	0.74	3.09	2.68	0.91
Al <sub>2</sub> O <sub>3</sub>	0.17	0.25	1.82	3.04	3.26	5.68	6.11	7.71	13.5
Cr <sub>2</sub> O <sub>3</sub>	0.03	<0.03	0.08	<0.03	0.03	<0.03	0.03	0.03	<0.03
MgO	19.8	7.58	14.6	0.36	8.29	7.80	1.87	2.31	0.15
CaO	29.3	43.7	23.5	41.3	16.2	12.9	2.55	2.73	0.23
FeO	1.88	1.71	7.63	2.90	12.1	8.19	15.5	10.1	2.31
MnO	0.90	0.18	0.26	0.07	0.32	0.16	0.07	0.11	<0.05
ZnO	<0.06	<0.06	<0.06	0.08	<0.06	0.07	<0.06	<0.06	<0.06
SrO	0.14	0.11	0.12	0.04	0.06	0.04	<0.04	<0.04	0.14
BaO	<0.06								
Na <sub>2</sub> O	0.19	0.65	1.81	1.22	2.85	5.98	9.26	8.45	7.62
K <sub>2</sub> O	0.04	<0.03	1.28	2.23	1.90	0.14	1.90	0.95	1.47
total	53.2	58.2	65.5	68.0	70.4	75.5	91.3	89.4	98.0

**Table 11:** Microprobe analyses of inter-granular sedimentary matrix. Silica content increasing from the left to right.

heavy mineral load of rivers from more distally located areas.

### V. Carbonatitic juvenile lapilli:

Juvenile lapilli represent two chemically distinct magmatic groups, i.e. calcicarbonatites and magnesiocarbonatites. Within the surrounding carbonatitic Gross Brukkaros Volcanic Field of the Gibeon Province calcicarbonatitic compositions are known only from one single location (dyke between vent A1 and vent-goup F, 1 mile west of Brukkaros; Janse, 1969; Kurszlaukis and Lorenz, 1992; Kurszlaukis, *in prep.*). The source of these calcicarbonatitic lapilli beds may be one or several centrally located diatremes now buried by the sedimentary fill of the Brukkaros depocentre. This would be consistent with a shallow magma reservoir located beneath Gross Brukkaros from which calcicarbonatites originated by a differentiation process and decomposition of dolomite from magnesiocarbonatites. They should preferentially be found in diatremes tapping the topmost parts of the reservoir, which would be located in the centre of the structure.

### VI. Metasomatic-hydrothermal alteration and cementation of the Brukkaros sediments:

Miller (pers. comm., 1992) interprets the greenish-grey pebble-sized fragments observed at Brukkaros as products of fenitization within carbonatitic diatremes before eruption. We interpret the greenish-grey lapilli from the western ‘crater’-rim also as products of metasomatic alteration of previous calcicarbonatitic lapilli, based on our microscopic and microanalytical observations. It appears unlikely that any secondary growth of very fine aegirine would have been restricted to the lapilli without also growing simultaneously in the matrix, so that predepositional fenitization as suggested by Miller is indicated.

Nevertheless post-depositional, *in-situ* metasomatic alteration also occurred. Strong evidence comes from euhedral aegirine (Fig.7) and albite overgrowths on

individual grains which were rounded during sedimentary transport. This alteration firstly involves growth of aegirine and Naand K-feldspar from and reaction with Na-, K-, Nb- and Fe-rich fluids. Feldspars with intermediate compositions are rare, which indicates that the fenitization has taken place below the crest of the feldspar solvus of 550°C (Le Bas, 1987). The small haematite stained dolomite rhombohedra may have grown simultaneously. This early metasomatic event was followed secondly by crystallization of quartz, barite and zeolite from hydrothermal solutions (see also Miller and Reimold, 1987).

These alteration events are not strictly separated, as shown for example by simultaneous crystallization of fine aegirine needles and quartz cement. Euhedral barite within quartz veins suggests that barite crystallized before quartz, but simultaneous growth of quartz and barite is also apparent. Crystallization of calcite in most cases seems to follow cementation by quartz. Euhedral calcite may, however, also be included in quartz veins.

The effects of hydrothermal alteration reached far beyond the Gross Brukkaros complex, since barite and quartz veins can be observed more than 10 km away.

In summary, the petrographic and chemical characterization of the Brukkaros beds does not produce any evidence for the presence of pyroclastic breccias or microbreccias (Rogers, 1915; Janse, 1969): On the contrary this supports the model of Stachel *et al.* (1993, 1994), who suggest an exclusively epiclastic origin of the Brukkaros beds with deposition in a synsedimentary subsiding calderalike depocentre. The metasomatic-hydrothermal alteration of the Brukkaros sediments supports the hypothesis of a shallow magma reservoir located centrally beneath the caldera-structure. The presence of calciocarbonatitic lapilli only within the Brukkaros caldera itself also suggests the uppermost parts of the reservoir to be located centrally within the overall complex.

#### Acknowledgements

Roy Miller (Namcor) introduced Gross Brukkaros to us during the beginning of our fieldwork and generously made available his previous petrographic research on these rocks. Volker Lorenz (Würzburg) contributed much to the geological understanding of the Gross Brukkaros structure and, together with Martin Okrusch, initiated the research project in the Gibeon Province. The microprobe analyses were carried out with the help of Uli Schüssler (Würzburg). We also wish to thank the Namibia field parties of 1990-93 for their valuable contributions. The comments and suggestions of Roger Smith (Cape Town) and a second reviewer are gratefully acknowledged.

Financial and technical support for the project by the Deutsche Forschungsgemeinschaft, Würzburg University, and the Geological Survey of Namibia are gratefully acknowledged. I.S. received sabbatical funding from

the Alexander von Humboldt Stiftung and funding in the field from the University of the Witwatersrand.

#### References

- Banno, S. 1959. Aegirineaugites from crystalline schists in Sikoku. *J. Geol. Soc. Japan*, **65**, 52-657.
- Clark J.R. and Papike, J.J. 1968. Crystal-chemical characterization of omphacites. *Am. Mineral.*, **3**, 840-868.
- Davies, G.R., Spriggs, A.J., Nixon, P.H. and Rex, D.C. 1991. A non cognate origin for the Gibeon kimberlite megacryst suite. *CPRM Spec. Publ.*, **2/91**, 63-65.
- Droop, G.T.R. 1987. A general equation for estimating Fe<sup>3+</sup> concentrations in ferromagnesian silicates and oxides from microprobe analyses, using stoichiometric criteria. *Geol. Mag.*, **51**, 431-435.
- Ferguson, J., Martin, H., Nicolaysen, L.O. and Danchin, R.V. 1975. Gross Brukkaros: a kimberlite-carbonatite volcano. *Phys. Chem. Earth.*, **9**, 219-234.
- Janse, A.J.A. 1969. Gross Brukkaros, a probable carbonatite volcano in the Nama Plateau of Southwest Africa. *Bull. Geol. Soc. Amer.*, **80**, 573-585.
- Kelber, K.P., Franz, L., Stachel, T., Lorenz, V. and Okrusch, M. 1993. Plant fossils from Gross Brukkaros (Namibia) and their biostratigraphical significance. *Communs Geol. Surv. Namibia*, **8** (1992/93), 57-66.
- Keller, J., Brey, G., Lorenz, V. and Sachs, P. 1990. Urach, Hegau, Kaiserstuhl. *Excursion guide, IAVCEI 1990, Mainz*, 63 pp.
- Kurszlaukis, S. and Lorenz, V. 1992. Die Geologie der Karbonatitschlote und-Dykes im Bereich des Gross Brukkaros. *Zbl. Geol. Paläont.*, **3/4**, 240-242.
- Le Bas, M.J. 1987. Nephelinites and carbonatites. In: Fitton, J.G. and Upton, B.G.J. (eds.): *Alkaline igneous rocks*. Oxford, London (Blackwell), 53-83.
- Miller, R.McG. and Reimold, W.U. 1987. Excursion guide: Brukkaros Roter-Kamm Crater structures, SWA/Namibia. *Int. workshop on cryptoexplosions and catastrophes in the geological record, 25.6.-2.7. 1987*, 33pp.
- Poldervaart, A. and Hess, H.H. 1951. Pyroxenes in the crystallization of basaltic magma. *J. Geol.*, **59**, 472-489.
- Reid, D.L., Cooper, A.F., Rex, D.C. and Harmer, R.E. 1990. Timing of post-Karoo alkaline volcanism in southern Namibia. *Geol. Mag.*, **127**, 427-433.
- Rogers, A.W. 1915. Geitzi/Gubib, an old volcano. *Trans. Roy. Soc. S. Afr.*, **5**, 247-258.
- Stachel, T., Lorenz, V., Stanistreet, I.G. and Miller, McG. 1992. Zur Vulkanologie und Sedimentologie des Gross Brukkaros. *Zhl. Geol. Paläont.*, **3/4**, 238-240.
- Stachel, T., Lorenz, V. and Stanistreet, I.G. 1993. Gross Brukkaros (Namibia)-a Cretaceous caldera with an epiclastic craterfill. *IAVCEI Canberra 1993, abstracts*, p.105.
- Stachel, T., Lorenz, V. and Stanistreet, I.G. 1994. Gross

- Brukkaros (Namibia)-an enigmatic crater-fill re-interpreted as due to Cretaceous caldera evolution. *Bull. Volcanol.*, **56**, 386-397
- Taylor, S.R. and McLennan, S.M. 1985. *The continental crust: its composition and evolution*. Oxford (Blackwell Scientific), 312 pp.
- Woolley, A.R. and Kempe, D.C.R. 1989. Carbonatites: nomenclature, average chemical compositions, and element distribution. *In*: Bell, K. (ed.): *Carbonatites: genesis and evolution*. London (Unwin Hyman), 113.